REVUE ROUMAINE DE GÉOPHYSIQUE

ROMANIAN GEOPHYSICAL JOURNAL

Tome 66, 2022–2023 **Volume 66, 2022–2023**

Contents / Sommaire

Rev. Roum. GÉOPHYSIQUE, **66**, p. 5–56, 2022–2023, București **htpps://doi.org/10.5281/rrg.2023.66**

OBSERVING CRUST DEFORMATION ALONG PECENEAGA-CAMENA FAULT

ZLĂGNEAN L., POMERAN M., BEȘUȚIU L.

[1] *Institute of Geodynamics Sabba S. Ştefănescu of the Romanian Academy*

The Baspunar permanent geodynamic station (BGO) is aimed at observing the slip rate along the well-known Peceneaga-Camena Fault (PCF). Its design is based on the idea that intensification of north-westward tectonic push from the Black Sea microplate may reflect in the slip increase along major faults within SE Carpathians foreland. As one of the major faults in the area, changes in the slip rate along PCF may serve as indicator of the increase of tectonic stress with its seismological consequences.

At BGO, two highly accurate Leica TC 1200–1201 total stations (±2ppm accuracy) measure and record every minute the distance between the PCF flanks. Raw observations are then corrected for the influence of atmospheric factors and averaged for a 5 minutes time span. To avoid the effect of fast changes in atmospheric parameters (mainly due to direct hit of the Sun rays), night records are taken into account only. Based on thus corrected and selected observations, slip rate is determined and compared with the amount of seismic energy released.

Key words: geodynamics, Peceneaga-Camena fault, Leica TPS 1201 total station, data acquisition software, atmospheric correction, slip rate, seismic energy.

1. INTRODUCTION

The Peceneaga Camena Fault (PCF) represents one of the most studied tectonic features of the Romanian territory. Ever since the beginning of the 20th century (e.g., Mrazec 1910, 1912; Macovei, 1912) PCF has been subject of numerous studies regarding its nature, in-depth extent and geodynamic evolution.

During the time, PCF has been considered in many ways, from a local reverse fault (Mrazec 1910; Macovei, 1912), or a large overthrust plane along which Proterozoic Green Schist of Central Dobrogea overthrust Northern Dobrogea Paleozoic deposits (Preda, 1964), to a strike slip fault (e.g., Săndulescu,1980; Hippolyte *et al*. 1996; Hippolyte, 2002).

Geological evidence shows a geodynamic evolution of this fault, with both right-lateral and left-lateral slip episodes (Pavelescu, Nitu, 1977; Săndulescu, 1980; Grădinaru, 1984; 1988; Seghedi, Oaie, 1995; Banks, Robinson, 1997). Scarce crustal earthquakes located on, or near the PCF plane, with strike-slip focal mechanism suggest that the fault might be still active.

It should be stressed that seismic tomography (Martin *et al*., 2006) has revealed PCF as a major lithospheric contact between Moesian Micro-Plate (MoP), and East European Plate (EEP).

Basically, BGO was designed and built up based on the geodynamic model proposed by Beşuţiu and Zugrăvescu (2004), Beșuțiu (2009) to monitor changes in the tectonic stress in the SE Carpathian foreland based on the observation of PCF slip rates.

The appropriate location of the observatory had to satisfy several major conditions like:

- a correct identification of the fault track (based on careful geological/geophysical investigations),
- adequate location on its flanks for emplacing the distance measuring instruments as well as their reflectors; instruments should run in conditions of local stability and best available accuracy,
- secure circumstances for functioning (power supply and backup source, available connection to internet, and permanent guard for observatory devices). All the above-mentioned conditions were encountered in the village of Fântâna Mare, commune of Ciucurova (Tulcea county) where the permanent station was set up (Figure 1).

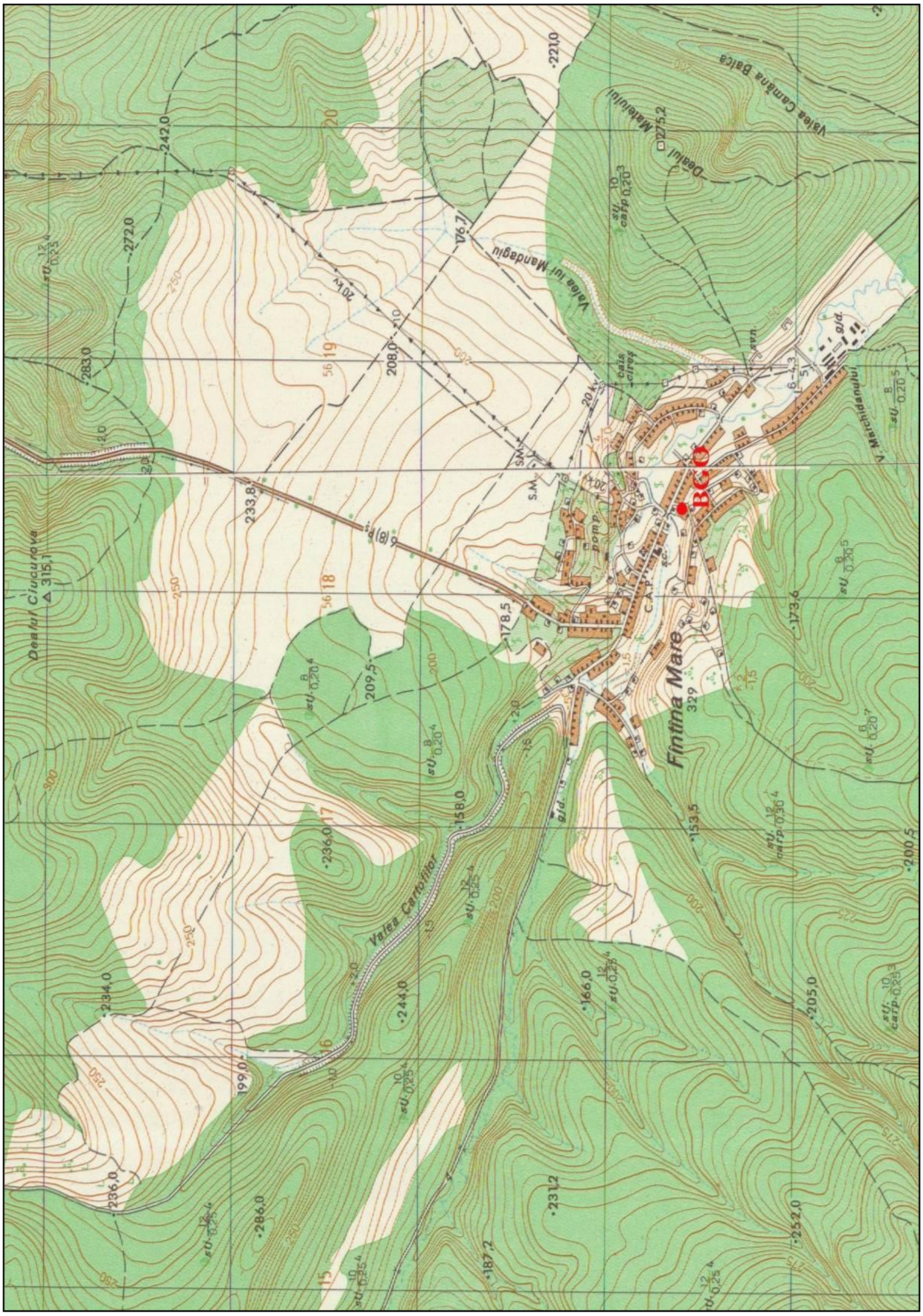

Figure 1 – Location of the Baspunar Permanent Station (BGO). Detail from the topographic map (scale 1:25.000). Approximated coordinates: latitude 44º51’ 30” N, longitude 28º29’ 25” E.

2. TECHNICAL INFRASTRUCTURE

Two high-precision total stations, Leica TPS 1200 (λ=780 nm) and TPS 1201 (λ= 658 nm) are placed on stable concrete pillars embedded on the southern flank of PCF, in the Proterozoic Green Schists of Central Dobrogea along with a WS2355 weather station for monitoring the atmospheric parameters.

The two total stations point towards two reflectors located on the other side of the fault, on the Jurassic deposits of Northern Dobrogea folded belt, at approximately 300 m (for the reflector placed on the pillar in front of the old school), respectively 350 m (for the reflector located on the wall of the church) (Figure 2).

Figure 2 – The infrastructure of the Baspunar Permanent Station (BGO).

3. IMPROVING THE ACCURACY OF DATA ACQUISITION

Leica TPS total stations come from the manufacturer with some internal software for data acquisition aimed at specific precision and speed. Among them, mentions should be made to the **Tracking mode** specialized in fast and continuous monitoring at the expense of precision and the **Standard IR mode** for high-precision measurements which is 3 times more accurate, but 4 times slower than the **Tracking mode**.

Given the peculiarities of the monitoring process, and especially the expected small changes in the fault slip, there has been a need to carry out both continuous observations, and, at the same time, very precise measurements. Therefore, the permanent goal was to improve measurements' conditions and precision continuously and substantially through several ways (such as improving data acquisition or post-processing of time series data).

The increase of data acquisition accuracy was achieved by implementing a new version of acquisition software developed in collaboration with colleagues from the Technical University of Civil Engineering of Bucharest.

The software has been designed and implemented by Dr. Marin Plopeanu from the Faculty of Geodesy and has allowed us to acquire data of high accuracy of the **Standard IR mode** at the speed of the **Tracking mode**.

The software is a stand-alone program, which includes 4 main sections:

1. The connection between the PC and the total station,
2. Command via PC of measurements in Standard IR mode,
3. Execution of repeated code sequences, at the measurement frequency set by the user,
4. Writing the results of observations in external files, easy to be transmitted for processing.

Figure 3 shows the way the data were improved by using the new acquisition software.

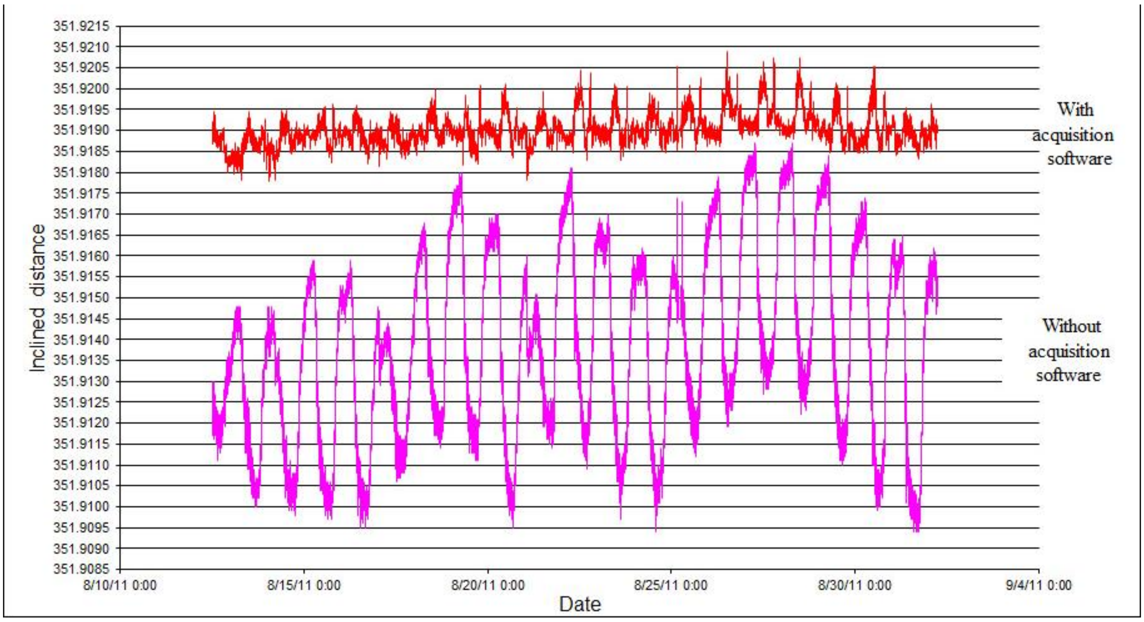

Figure 3 – Data improvement as a result of using the acquisition software.

4. DATA POST PROCESSING

Raw data post processing aims to apply some corrections in order to ensure the comparability of the results.

A first measure considered seeks to reduce the influence that atmospheric factors have on geodetic observations and consists in applying specific atmospheric refraction corrections (distances should be corrected for the actual refractive index of air along the measured line, between instrument and reflector). The formulae applied are provided by the manufacturer:

$$S_d corr = (s_d meas \text{ x } n0) / n_A$$

where $S_D corr$ is the corrected distance, $S_D meas$ is the measured distance and n_0 and n_A have the following forms:

$$n_0 = 1 + \frac{n_g - 1}{1 + 0.003661 * 12} * \frac{760}{760} - \frac{5.5 * 10^{-8}}{1 - 0.003661 * 12} * 4.58 * 10^{\frac{12a}{b+12}} * \frac{60}{100}$$

$$n_A = 1 + \frac{n_g - 1}{1 + 0.003661 * t} * \frac{PmmHg}{760} - \frac{5.5 * 10^{-8}}{1 - 0.003661 * t} * 4.58 * 10^{\frac{at}{b+t}} * \frac{r}{100}$$

n_g is a constant of the instrument we use, in our case Leica Total station models TPS 1200 and TPS 1201 and is provided by the following formula:

$$n_g = 2876.04 + 3 * \frac{16.288}{\lambda^2} + 5 * \frac{0.136}{\lambda^4} 10^{-7} + 1$$

And a=7.5, b= 237.3 and λ = 658 or 780 nm wavelength of the beam (specific for each instrument type).

Other symbols are weather related data at the moment of distance measuring: t[°C] temperature, r [%] relative humidity, P_{mmHg} the absolute pressure

A second measure aimed at removing the influence of the deformations produced by direct solar radiation on the support on which the station's reflector is installed. This deformation is uneven throughout the day depending on the angle of incidence of the sun's rays. For this reason, in studying the dynamics of the Peceneaga-Camena fault (PCF), daily averages and only the nocturnal recordings, between the time of sunset and sunrise, were taken into account.

5. DATA POST-PROCESSING SCRIPTS

The idea of developing scripts for processing raw data came from the current trend of increasingly automation within technology. This project started as a learning project for a junior colleague but after many years became a project to whom many people have contributed.

The purpose of the data processing scripts is to automate as much as possible the work needed to transform the field observed data into data corrected by the influence of changes in the atmospheric conditions. The input parameters mainly represent atmospheric factors (air temperature, atmospheric pressure and humidity), and the inclined distance measured between the flanks of the PCF. A full list of the input and output parameters are in Table 1.

The current process of data acquisition involves two human operators, one at the BGO, and the other at the computing center. The field operator is responsible for keeping the hardware in operation and with the daily data transmission to the center. The center operator is responsible for processing the data. All the phases of the process are listed in table 2 and are performed daily (weekdays), Mondays with the data over the week-ends.

Phases 1 and 2 are performed by the field operator. Phase 1 is accomplished by means of the new Laptop 2TPS software previously described. Phases 2 and 3 are facilitated by a well-known web application used to synchronize files across the internet (Dropbox). Phases 3 to 6 are performed by the center operator, some of them being automated. Phase 4 is performed with a click of the mouse and can either process one day or a month, one day at the time. Also, Phase 4 was adapted to run on Windows OS (operating system) with the aid of Vagrant and VirtualBox. Phase 4 consists of a collection of scripts and its sub-phases are described in Table 3.

Table 1

Input and output parameters

#	Type	Role	Description	Observation
1	Input	Primary	Raw meteo data file	Recorded at 300s intervals
2	Input	Primary	Raw telemetry data file	Recorded at 300s intervals
3	Input	Primary	Formulae and their parameters	
4	Input	Secondary	Current date	From the running computer
5	Input	Secondary	Date of processed day/month	One month interval
6	Input	Secondary	Raw files path on the processing computer's file system	Dropbox; rarely changed
7	Input	Secondary	Output files path on the processing computer's file system	
8	Input	Secondary	Raw files naming pattern	Human operator names files
9	Input	Secondary	Timestamps format inside the raw files	
10	Input	Secondary	Number of seconds needed to shift the time stamps by	Human operator records interval
11	Input	Secondary	Processed file: raw meteo and telemetry data along with corrected distance	Each record at predefined timestamp 300s apart from the next/previous: 00:00, 00:05, etc. regardless of inherent input data drift

Table 2

Phases in which raw data are transformed into meaningful data

	Description	Running OS	Observation
Phase 1	Input records are assembled in files	Windows	automatic
Phase 2	Input files are uploaded in the cloud	Windows	human operator
Phase 3	Input files are downloaded from the cloud	Windows or Linux	automatic
Phase 4	Processing raw data for a range of days	Linux	automatic; can be Linux guest on Windows host
Phase 5	Diurnal data filtered put from phase 4 processed files; compute medians, regression slope	Windows	human operator; MS Excel
Phase 6	Phase 5 medians, regression slope stored as single record for the sunset date	Windows	human operator; MS Excel

Table 3

Automated steps of data processing

	Description	Observation
Phase 4.1	Create folders for the processed day	
Phase 4.2	Prepare input files for the processing scripts	
Phase 4.3	Compensate for hardware clocks drifting apart by shifting the records of one file	
Phase 4.4	Edit the processing scripts to work on the processed day	
Phase 4.5	Extract the data relevant to the processed day	
Phase 4.6	Synchronize records to exact 300s intervals by approximation	
Phase 4.7	Records the lack data, are replaced with only timestamps	Useful for phase 5
Phase 4.8	Reorder the columns	
Phase 4.9	Apply the formulae and write the output	Output file is in the folder from phase 4.1

After applying the atmospheric correction formulae in phase 4, diurnal data is discarded and the night records are mediated in phase 5. All the nocturnal data is condensed in a single record in phase 6.

Phases 4.1 and 4.2 mainly prepare the data and populate secondary input variables (table 1). Phase 4.3 is an application (Pomeran, 2022) designed to compensate if the hardware clocks of weather station and Total station drift apart. Phases 4.4, 4.5, 4.8 and 4.9 are remnant from the early days and the respective code required minimal maintenance. Phases 4.6 and 4.7 were developed later and make use of the generic mapping tools (Wessel, P. *et al.*, 2019). It may seem that phases 4.3 and 4.6 are redundant but in the later phase is assumed that the time stamps of the input files are synchronized. The work on these scripts continues, as software bugs occasionally appear, also its goal is not yet achieved.

Figure 4 shows improvement of results after data processing following the above-mentioned listed steps.

6. SOME RESULTS

We currently benefit from continuity in monitoring the dynamics of the Peceneaga-Camena fault for about a decade. Figures 5 to 13 show variation of the corrected and daily averaged slope distances between the PCF flanks versus atmospheric parameters recorded at BGO.

There is an overlap of both daily and seasonal variations of the considered parameters (especially temperature). After processing, most of the effects of daily and seasonal variations of the atmospheric parameters are removed from our recordings.

The averaged slope distance variations show a behavior of strike slip type with alternating episodes of the fault sliding. The problem that we posed first and foremost was whether through all the actions that we undertook and that we previously presented, we managed to eliminate the influence of atmospheric parameters, and here we are referring in particular to the temperature, the most influential factor. From the following graphs (Figure 14) it can be seen that a direct, clear connection cannot be established between the corrected slope distances and temperature variations, so we can appreciate that recorded variations are mostly due to geodynamic causes (Figure 14).

Another question we asked ourselves when BGO was founded, was whether and to what extent there is a connection between the possible sliding on the PCF and the seismic activity in the foreland of the Carpathians arc bend.

Figure 15 shows the earthquakes epicenters of the Vrancea seismic zone and of the Carpathian foreland between 2014 and 2022. Black dots are the epicenters of crustal earthquakes and the red ones of intermediate earthquakes (Figure 15).

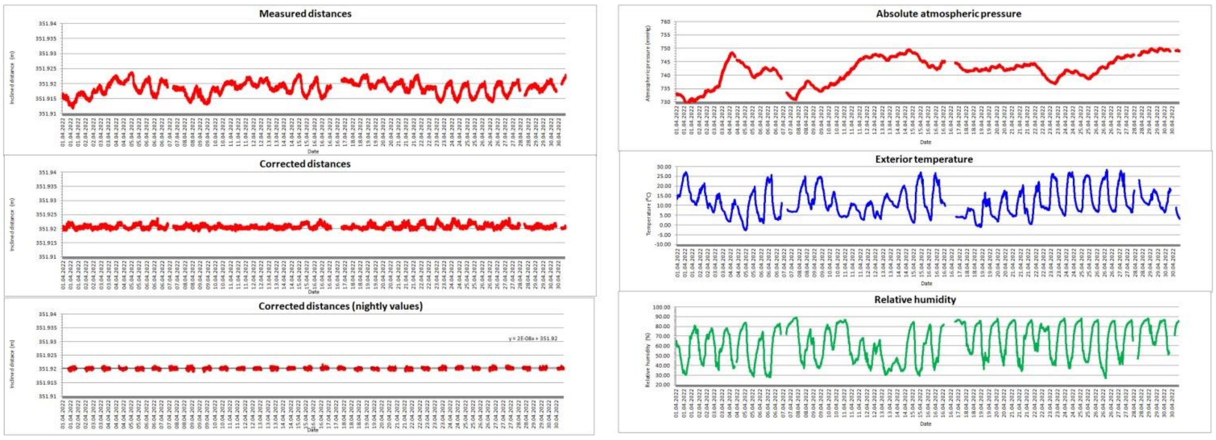

Figure 4 – Measured/corrected distances (left) *versus* atmospheric parameters (right).

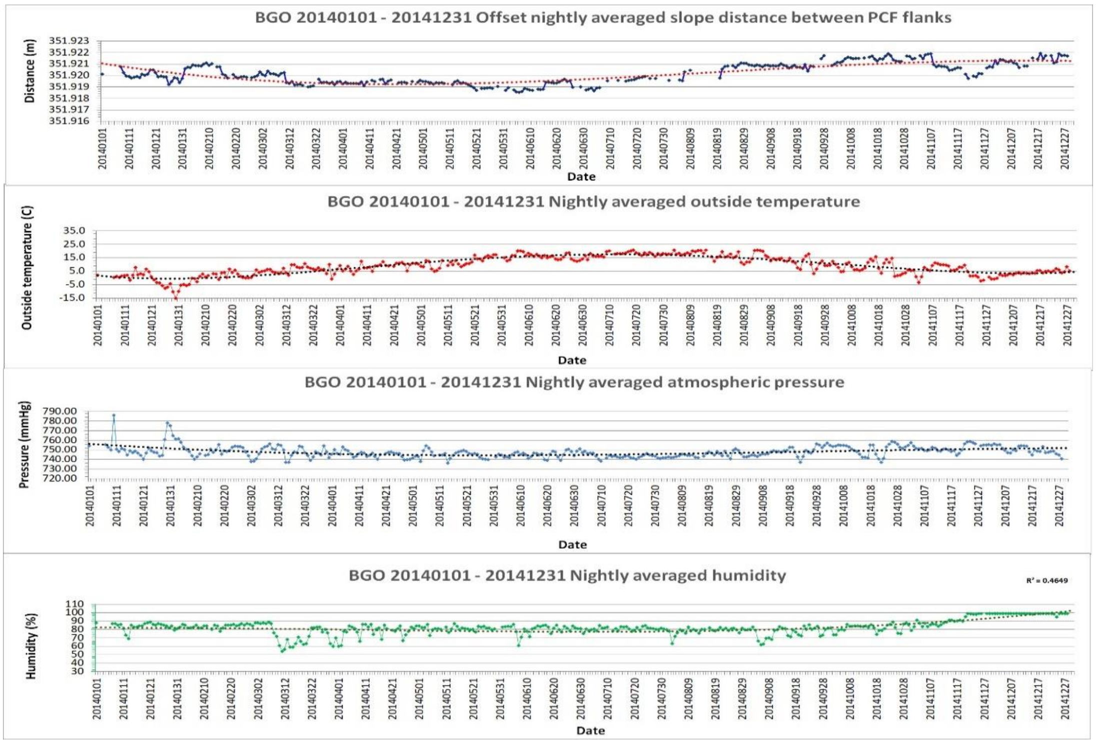

Figure 5 – 2014 Offset nightly averaged slope distance between PCF flanks *versus* nightly averaged atmospheric parameters.

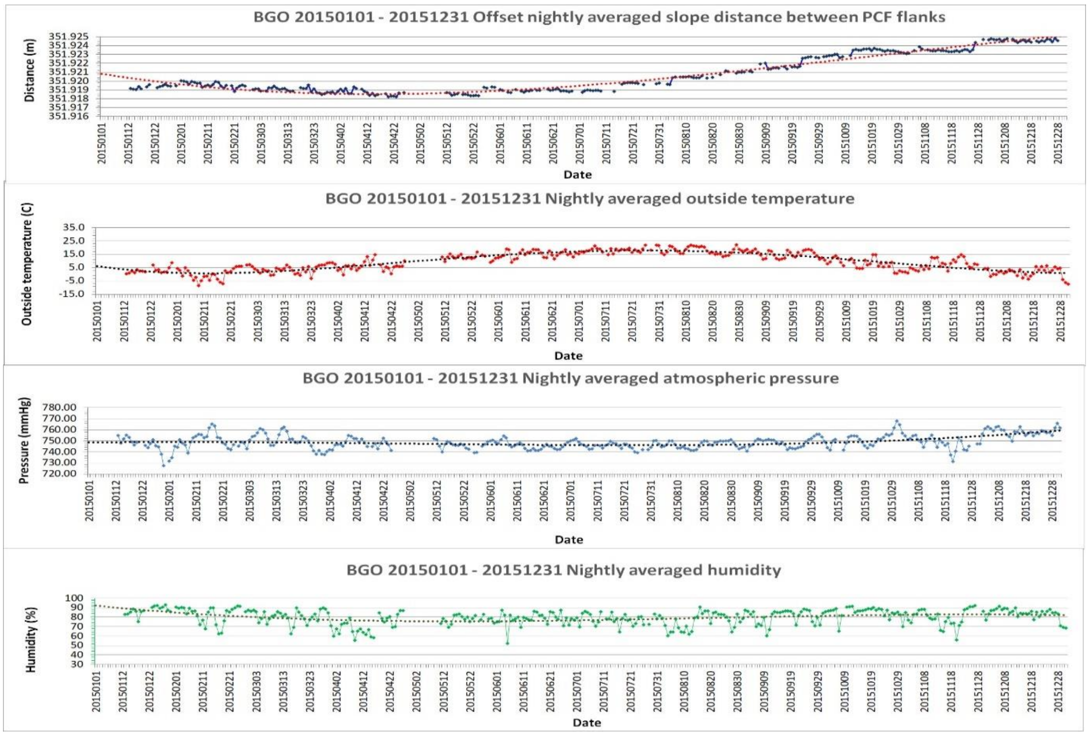

Figure 6 – 2015 Offset nightly averaged slope distance between PCF flanks *versus* nightly averaged atmospheric parameters.

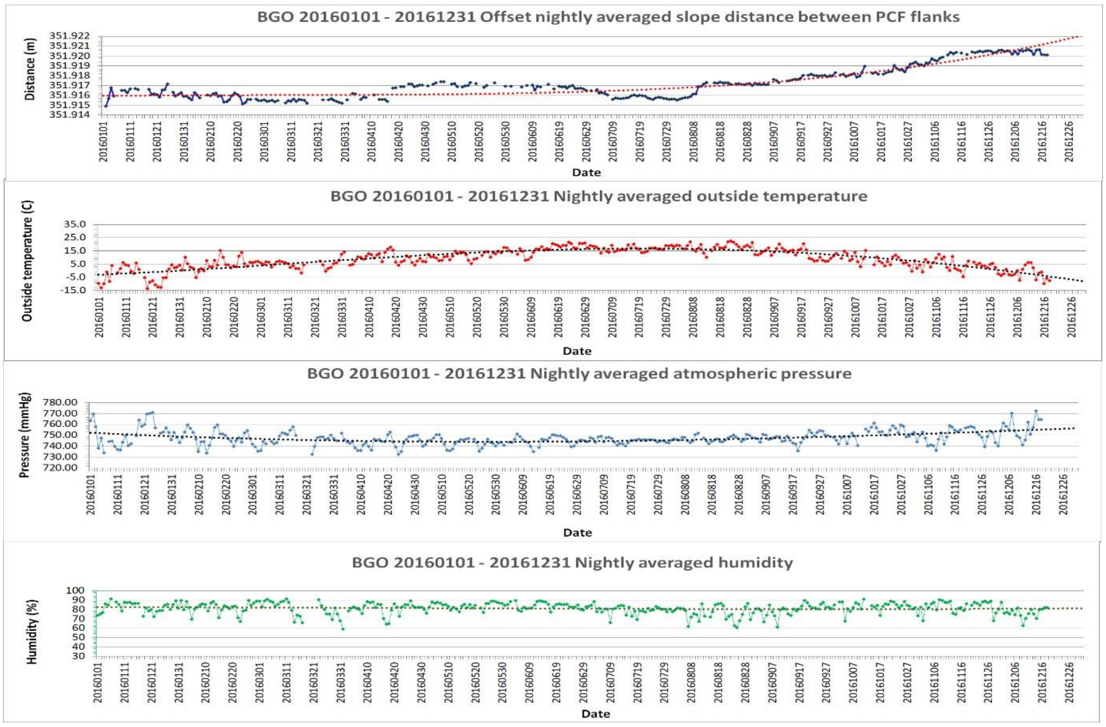

Figure 7 – 2016 Offset nightly averaged slope distance between PCF flanks *versus* nightly averaged atmospheric parameters.

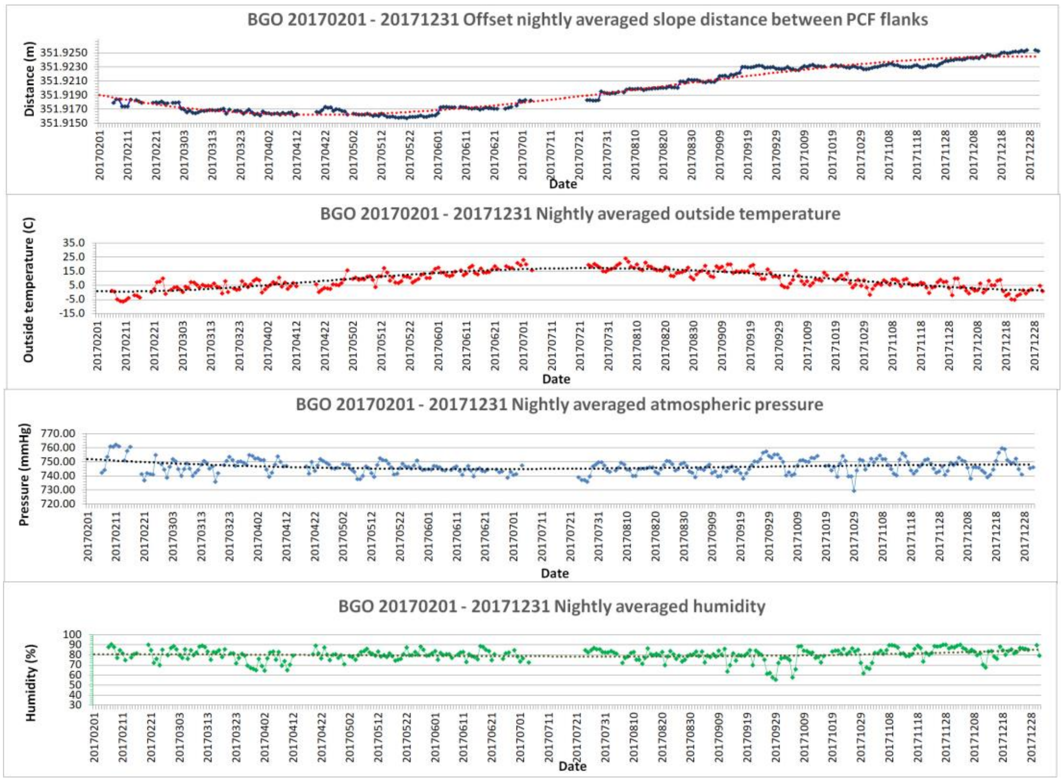

Figure 8 – 2017 Offset nightly averaged slope distance between PCF flanks *versus* nightly averaged atmospheric parameters.

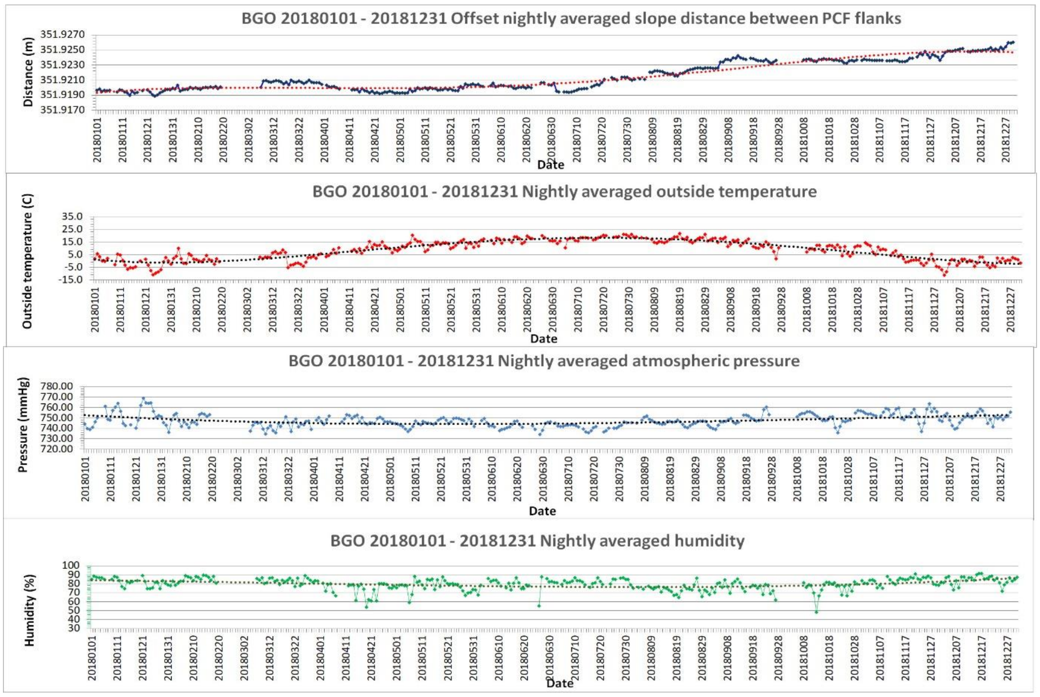

Figure 9 – 2018 Offset nightly averaged slope distance between PCF flanks *versus* nightly averaged atmospheric parameters.

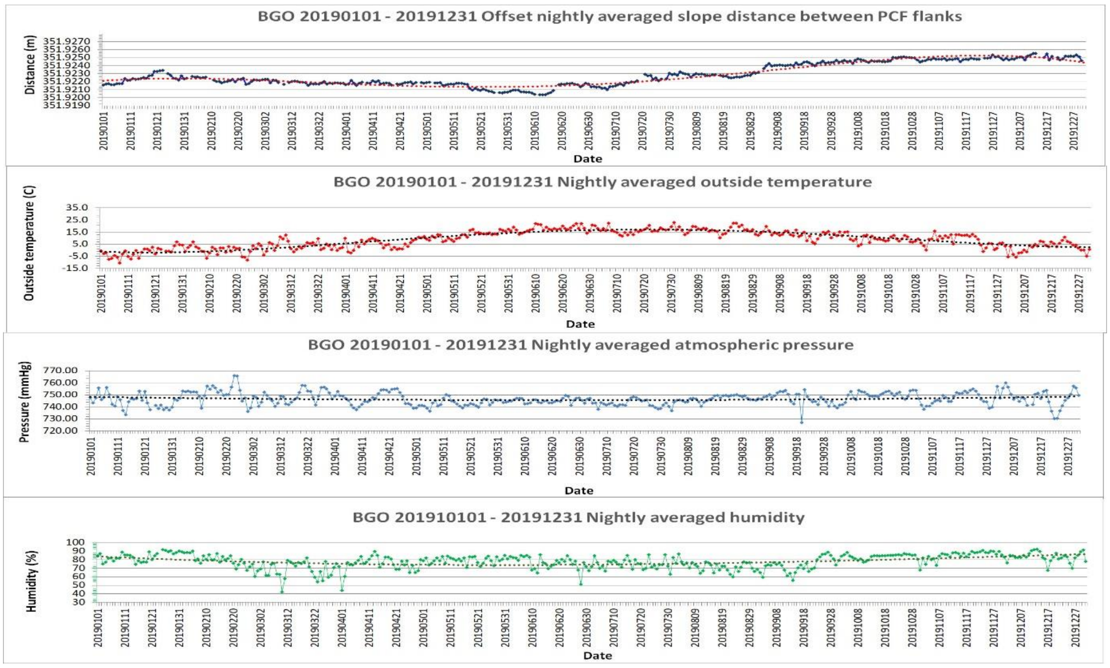

Figure 10 – 2019 Offset nightly averaged slope distance between PCF flanks *versus* nightly averaged atmospheric parameters.

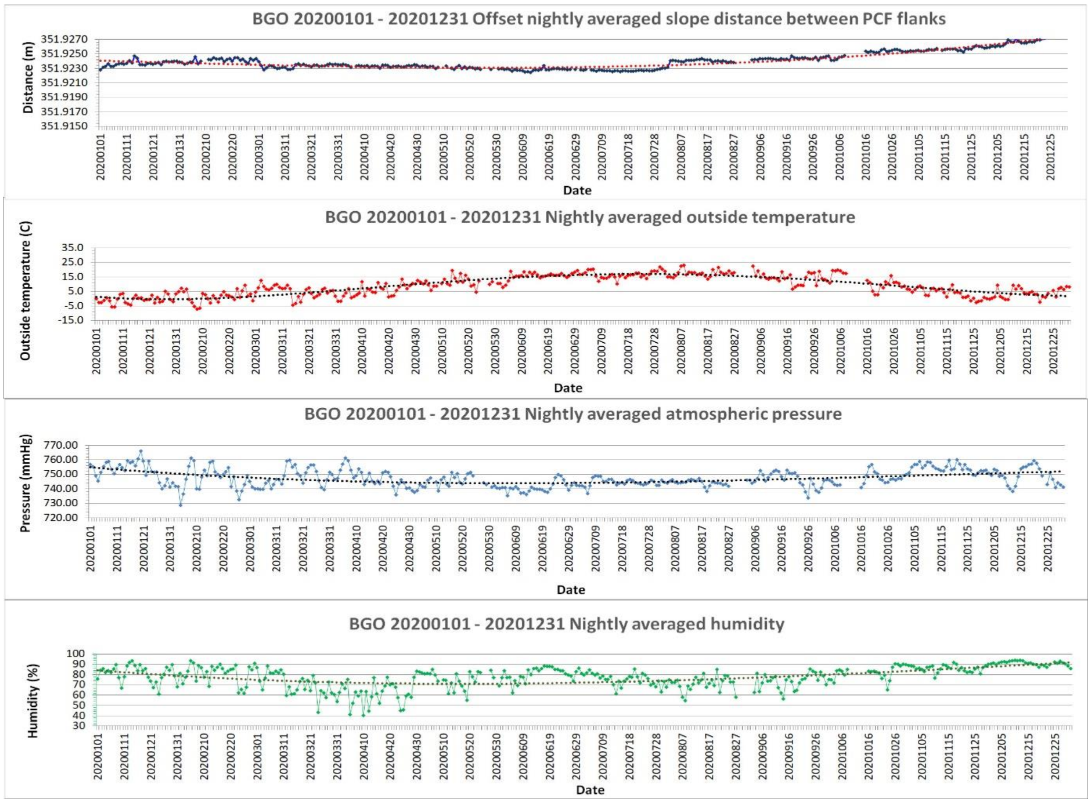

Figure 11 – 2020 Offset nightly averaged slope distance between PCF flanks *versus* nightly averaged atmospheric parameters.

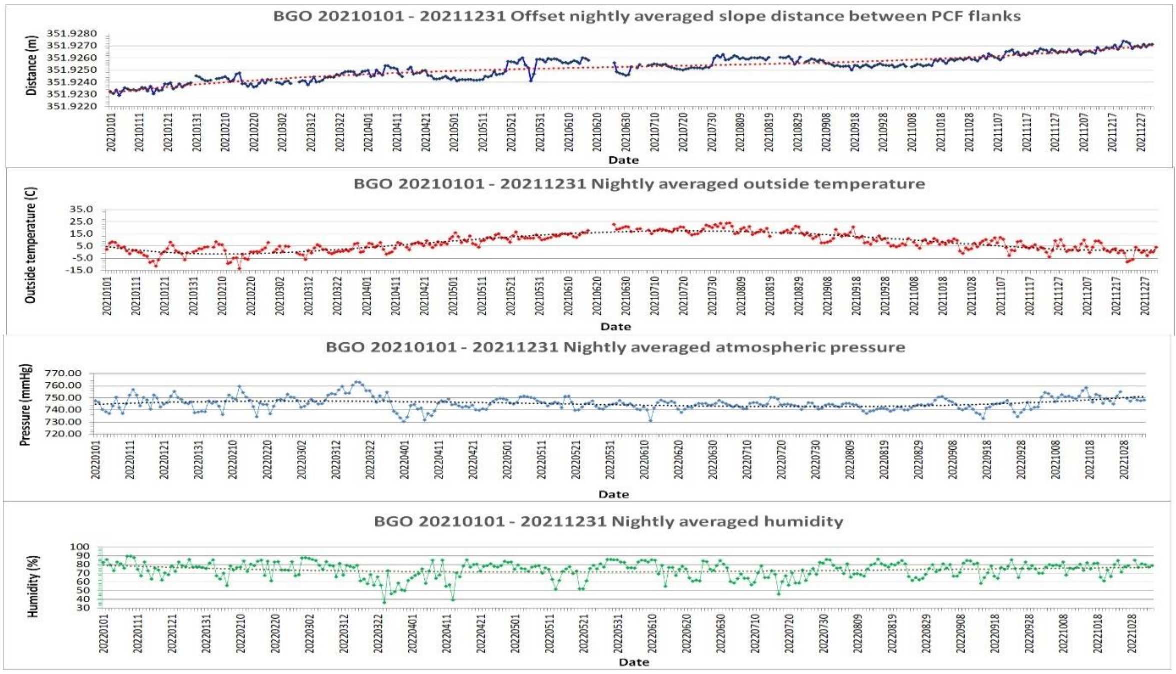

Figure 12 – 2021 Offset nightly averaged slope distance between PCF flanks versus nightly averaged atmospheric parameters.

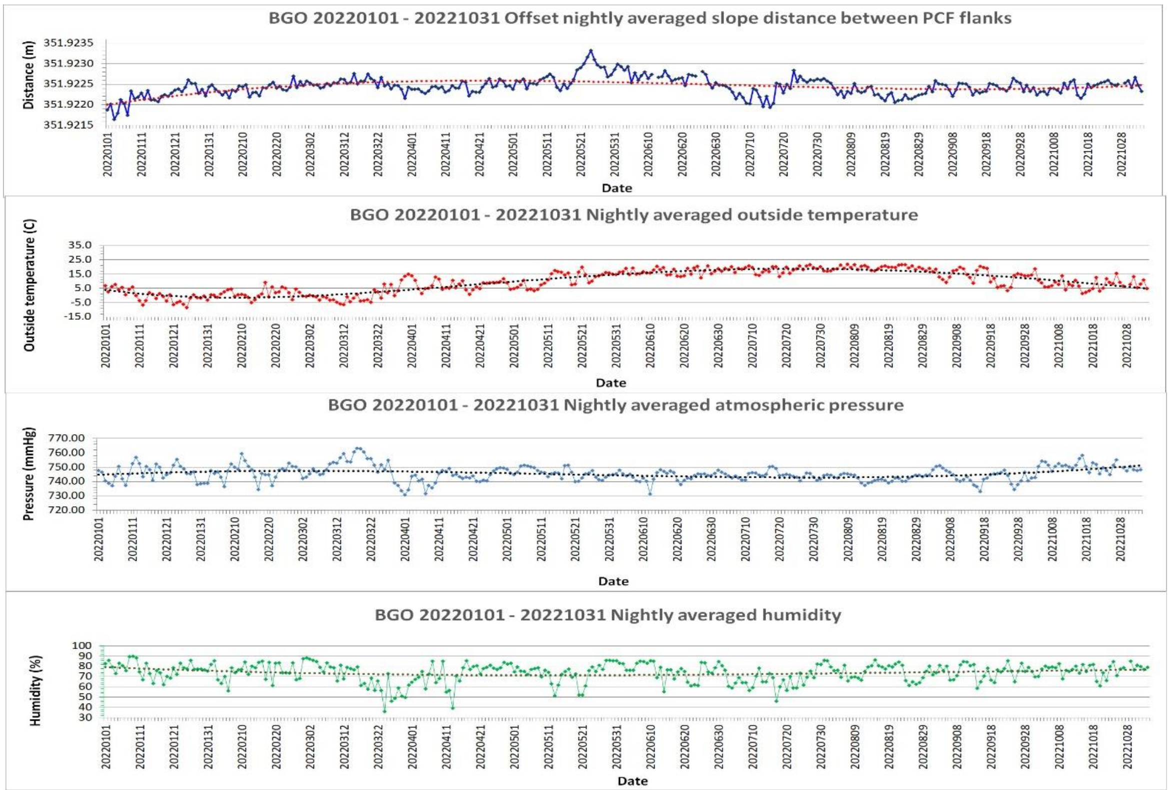

Figure 13 – 2022 Offset nightly averaged slope distance between PCF flanks *versus* nightly averaged atmospheric parameters.

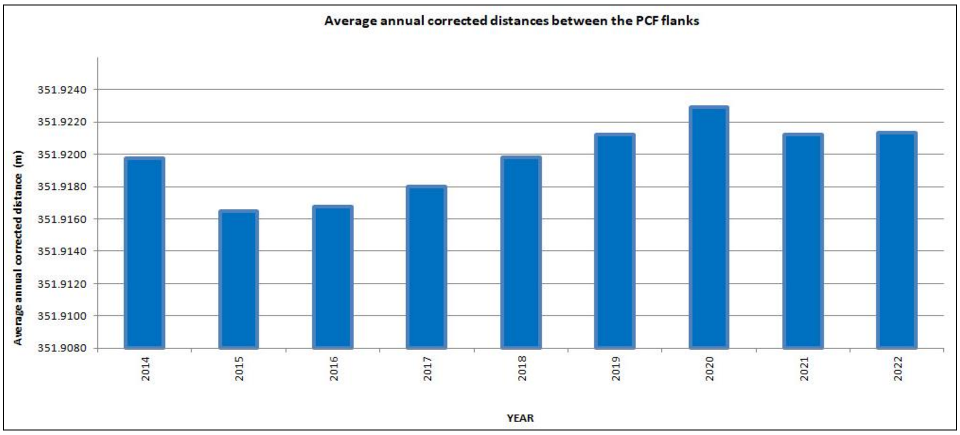

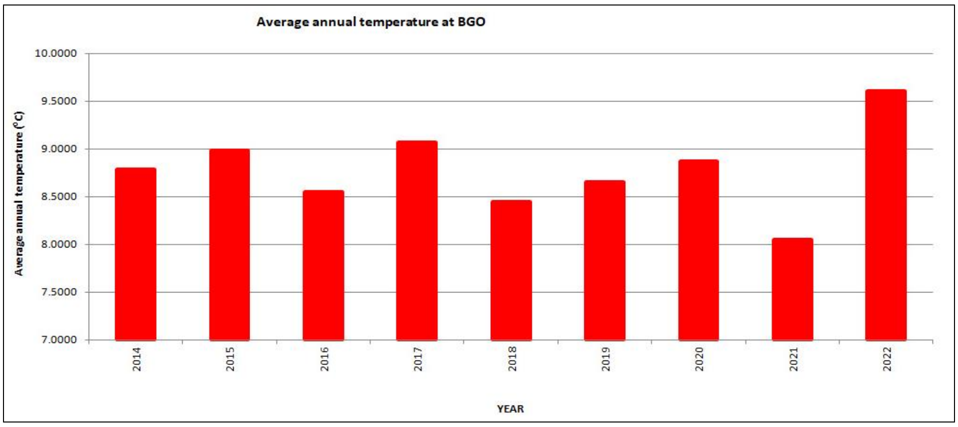

Figure 14 – Average annual corrected distances *versus* average annual temperature recorded at BGO.

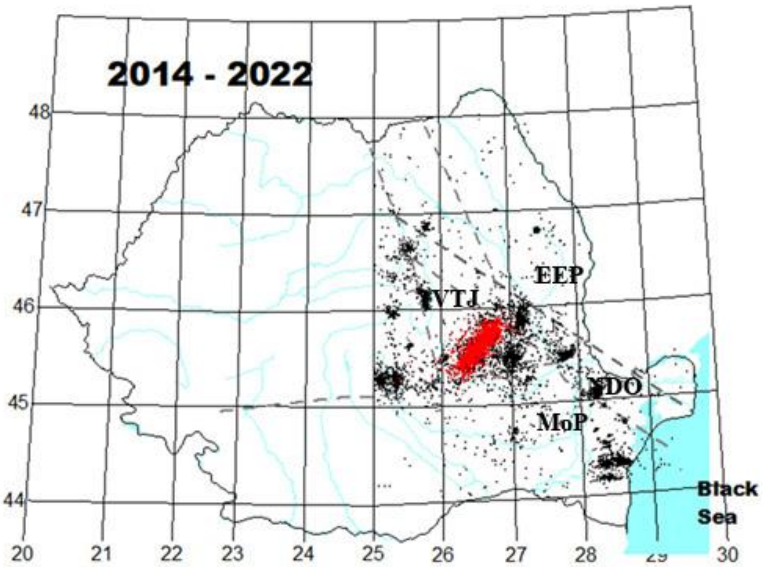

Figure 15 – Seismicity recorded within the Carpathian Bending Arc and its foreland. VTJ-Vrancea Triple Junction, NDO-North Dobrogean Orogen, MoP-Moesian Plate, EEP-East European Plate (Beșuțiu L.,2009).
Red dots – Vrancea intermediate seismicity, black dots – custal seismicity.

Comparing the seismicity of each of the compartments in front of the Carpathians with the average corrected slope distances (Figures 16 and 17), it seems that the slips on the fault are best correlated with the crustal seismic activity in the northern Dobrogea compartment (NDO).

Last but not least it is worth mentioning one of the most representative cases regarding the behavior of the fault, which was caught in the recordings from 2013, when the Galați Izvoarele swarm of earthquakes occurred, and was previously presented in detail (Beșuțiu *et al*., 2019).

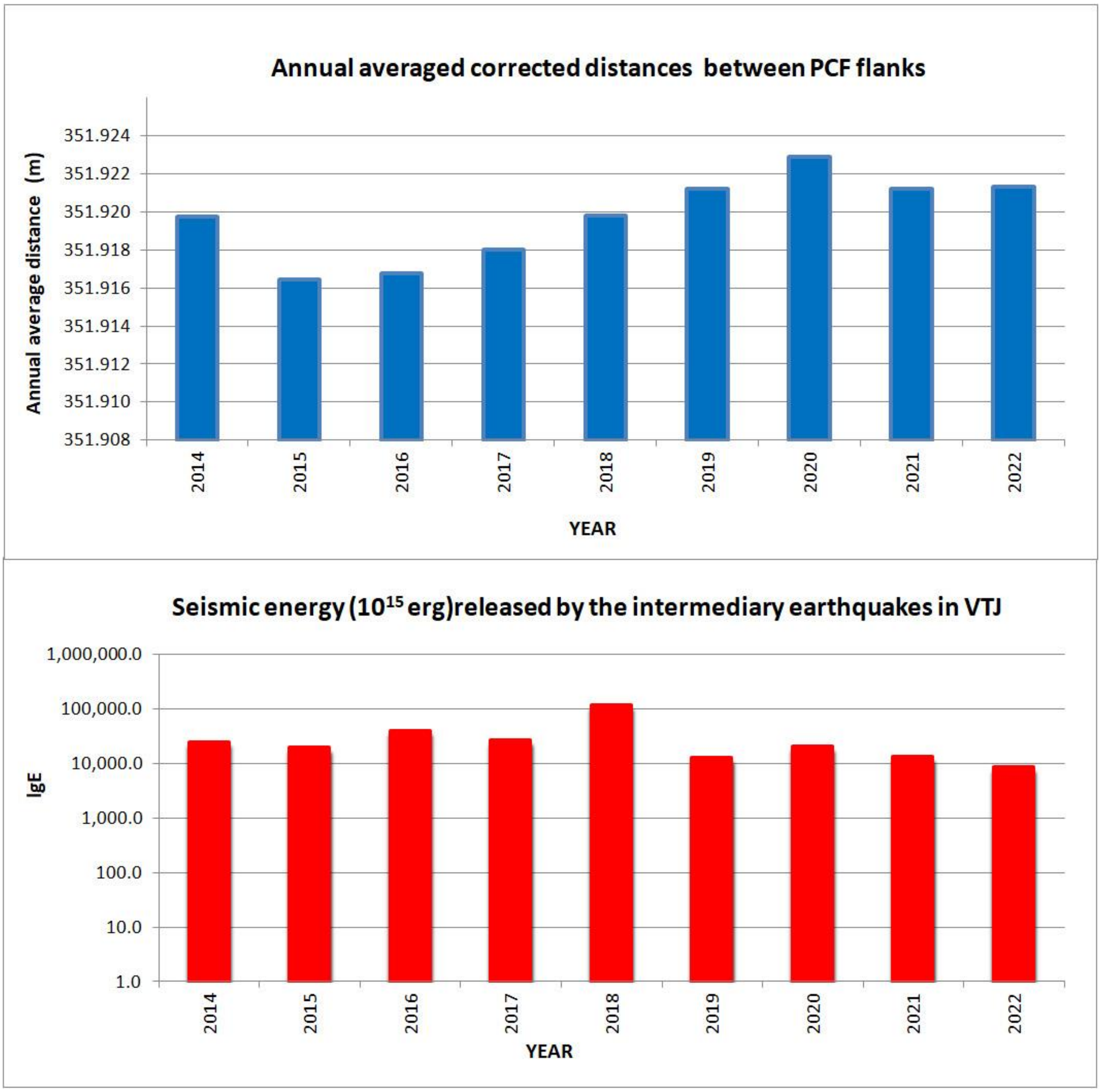

Figure 16 – PCF displacements versus seismic energy released by the intermediary earthquakes in VTJ.

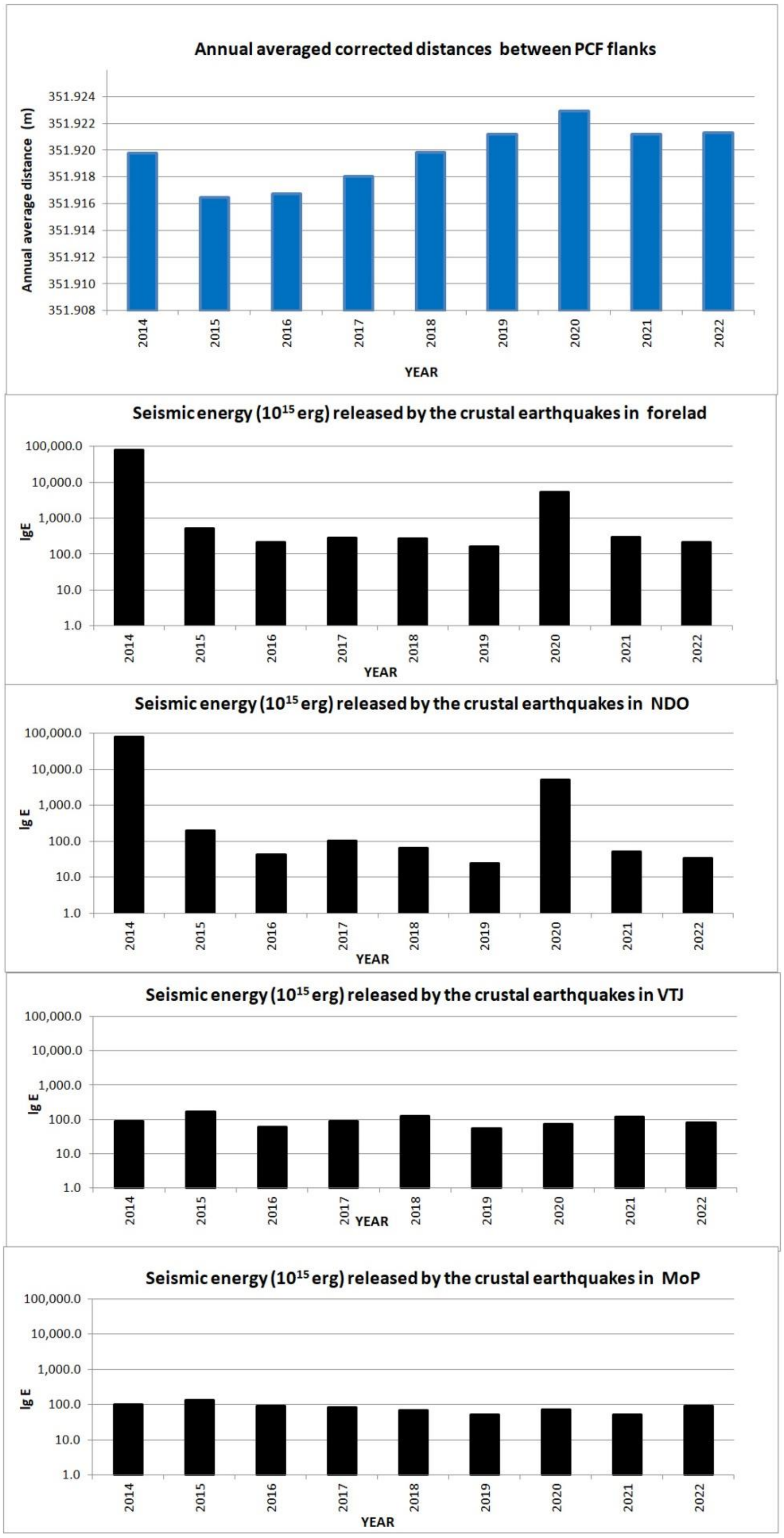

Figure 17 – PCF displacements *versus* seismic energy released
by the crustal earthquakes in Carpathian foreland.

REFERENCES

Banks C. J., Robinson A. (1997), *Mesozoic strike-slip back-arc basins of the western Black Sea region*. In A. G. Robinson (Ed.), Regional and petroleum geology of the Black Sea and surrounding region (Vol. 68, p. 53–62). Tulsa: AAPG Memoir

Beşuţiu L., Zugrăvescu D. (2004), *Considerations on the Black Sea opening and related geodynamic echoes in its NW inland as inferred from geophysical data interpretation*. Ukrainian Geologist, no.3, p. 51–60, Kiev.

Beşuţiu L. (2009), *Geodynamic and seismotectonic setting of the SE Carpathians and their foreland*. In: L. Beşuţiu (Ed.) Integrated research on the intermediate depth earthquakes genesis within Vrancea zone. Vergiliu Publ. House, p. 233–248.

Beşuţiu L., Diaconescu M., Zlăgnean L., Craiu A. (2019). *Structural and Geodynamic Ideas on the Galati-Izvoarele Seismic-Prone Area (Eastern Romania)*. Pure Appl. Geophys. **176,** 65–95, https://doi.org/10.1007/s00024-018-1956-0

Grădinaru E. (1984) - *Jurassic rocks of north Dobrogea. A depositional–tectonic approach*. Rev. Roum. Géol., Géophys. Géogr., 28, 61–72.

Grădinaru E. (1988), *Jurassic sedimentary rocks and bimodal volcanics of the Carjelari-Camena outcrop belt: evidence for a transtensile regime of the Peceneaga-Camena Fault*. Stud. Cerc. Geol., Geofiz. Geogr., Ser., Geol., Acad. Române, 33, 97–121, Bucharest.

Hippolyte J.C., Săndulescu M., Bădescu D., Bădescu N. (1996), *L'activité d'un segment de la ligne Tornquist-Teisseyre depuis le Jurassique superieur: la faille de Peceneaga-Camena (Roumanie)*. Comptes Rendus de l'Academie des Sciences Paris, Serie II. Sciences de la Terre et des Planetes, 323:1043–1050.

Hippolyte J.C. (2002), *Geodynamics of Dobrogea (Romania): new constraints on the evolution of the Tornquist–Teisseyre Line, the Black Sea and the Carpathians,* Tectonophysics 357, 33–53.

Martin M., Wenezel F., CALIXTO WORKING GROUP (2006), *High-resolution teleseismic body wave tomography beneath SE-Romania – II, Imaging of a slab detachment scenario*. Geophysical Journal International 164, 579–595.

Mrazec L. (1912), *Asupra liniei de încălecare Peceneaga-Camena* . D.S.Inst. Geol.Rom., III, p. 163–165.

Mrazec L. (1910.), *Distribuirea rocelor verzi în direcţiunea stratelor în care se găsesc*. D.S. Inst. Geol. Rom., II, p. 26–39.

Macovei G. (1912), *Observaţiuni asupra liniei de încălecare Peceneaga –Camena,* D.S.Inst.Geol.Rom, III, Bucuresti, p.155-163

Pavelescu L., Niţu G. (1977), *Le probléme de la formation de l'arc carpatho-balkanique*. Ann. Univ. Bucur. Geol. 26, 19–35.

Preda D.M., (1964), *Forelandul carpatic şi poziţia sa tectonică în cadrul structural-geologic al Europei (The Carpathian foreland and its position within the geological-structural setting of Europe)*. An. Com. Geol., XXXIII, (in Romanian) R.S.R., Bucureşti, p. 9–36.

Sandulescu M.(1980), *Analyse géotectonique des chaînes alpines situées autour de la Mer Noire occidentale*. Ann. Inst. Geol. Geofiz. 56, 5–54, Bucharest.

Seghedi A., Oaie G. (1995), *Palaeozoic evolution of North Dobrogea*. In: Săndulescu *et al*. (Eds), Field Guidebook, Central and North Dobrogea IGCP Project no. 369 Comparative evolution of PeriTethyan Rift Basins, Mamaia , 5–75.

Pomeran M. (2022), *Time shift* (Version 0.0.1) [Computer software].https://doi.org/10.5281/zenodo

Wessel P., Luis J. F., Uieda L., Scharroo R., Wobbe F., Smith W. H. F., Tian D. (2019), *The Generic Mapping Tools version 6*. Geochemistry, Geophysics, Geosystems, 20, 5556–5564. https://doi.org/10.1029/2019GC008515

*** – Leica TPS 1200 and 1201 User Manuals.

SHEAR-WAVE VELOCITY DATABASE – A KEY INPUT FOR SEISMIC SITE AMPLIFICATION MODELS IN BUCHAREST, CAPITAL OF ROMANIA

ANDREI BĂLĂ[1], DRAGOȘ TOMA-DANILA[1], CRISTIAN ARION[2]

[1] *National Institute for Earth Physics (INCDFP), 12 Călugăreni Str., Măgurele, Ilfov, Romania*
[2] *Technical University of Civil Engineering Bucharest (UTCB), 122–124 Lacul Tei Bd., sector 2, Bucharest, Romania*

The evaluation of seismic hazard at local scale, with the contribution of strong-motion data from a dense seismic network and insightful geological and geophysical data, is one of the key components in seismic risk mitigation. Significant efforts were made to record and predict the highly variable peak spectral amplification values of strong seismic motion in Bucharest, capital city of Romania, especially after the 4 March 1977 Vrancea earthquake with a moment-magnitude of 7.4, which resulted in 1424 victims in the city (90% out of the national total). Research was made to evaluate seismic site effects, as a result of the continuously growing dataset of seismic, soil-mechanic and elasto-dynamic parameters recorded in the field, but to this date there is no official microzonation map issued. In this paper we review studies referring to shear wave velocity (V_S) measurements in the area of Bucharest – as key input for seismic site amplification models and microzonation maps, selecting and reprocessing some data in order to obtain a homogenized database. This contains mean weighted V_S values for the uppermost 30 m, 50 m, 70 m and 100 m depth intervals. By mapping and interpreting the distribution of values we provide additional means for future microzonation studies, highlighting also the importance of using deeper than 30 m V_S measurements.

Key words: shear-wave velocity; site amplification; microzonation; seismic hazard; Bucharest.

1. INTRODUCTION

In local seismic hazard (microzonation) studies, the availability of accurate local determination of the shallow soil layers characteristics is very important in order to determine the local response under various seismic scenarios. The result of 1D, 2D and 3D modelling can reflect the local variability of the soil package, leading to the understanding of potential building damage and measures of seismic risk mitigation (Thitimakorn 2013). In large cities located on thick layers of sediments (such as Bucharest – capital of Romania), affected also by earthquakes with variable source parameters, detailed input data regarding geological and geophysical data but also real strong motion recordings (at surface and in boreholes) are important for determining relevant building design parameters. The largest amplification of the soil will occur at the lowest natural frequency or its fundamental frequency (Bălă *et al*., 2009a), which corresponds to the characteristic site period. In situ measurements of shear wave velocity (V_S) and soil thickness provide a direct measure of the characteristic site period. Seismic noise measurements are an accessible method and computed H/V spectral ratio can also provide a good indication on the fundamental frequency of the site. New seismic methods for measuring and determining V_S have been derived and tried in Bucharest in recent years.

Mean weighted shear-wave velocity in uppermost 30 m depth interval (   ) is considered by Eurocode 8 (European Committee for Standardization, 2004) and the Romanian Seismic Design Code P100–1/2013 (UTCB, 2013) to be usually a useful indicator in seismic hazard assessment – revealing areas with generic variations of average seismic velocities. However, for seismic site amplification models and nonlinear site response analyses in areas with thick layers of sediments such as most major cities,   might not reflect adequately the soil characteristics leading to significant amplification variabilities (Cioflan *et al*., 2009; Yordkayhun *et al*., 2015; Yaghmaei-Sabegh & Rupakhety 2020).

 htpps://doi.org/10.59277/rrgeo.2023.66.2

The city area of Bucharest presents geological conditions which, in the context of strong motion induced by intermediate-depth earthquakes in the Vrancea Seismic Source (occurring typically at 60–150 km located 130–190 km hypocentral distance away from the city), leads to significant local site amplification (Mărmureanu *et al*., 2016) and variability of parameters at surface and as such different damage distribution (Toma-Danila & Armaș 2017). Among the key geological features are:

- the absence of hard bedrock down to Cretaceous upper limit at 500–1500 m depth (Lăcătușu *et al*., 2007);
- an alternation up to 300 m of thick Quaternary sand and clay layers near surface;
- 3 main porous aquifer systems among the sand and clay layers;
- strong lateral heterogeneities and important vertical thickness variations of soft soil deposits and aquifers complicating the geologic structure.

Recent several studies (among which Cioflan *et al*., 2009, Bălă *et al*., 2014 and von Steht *et al*., 2008) have emphasized that V_S is important but must be known until deeper depths (of 100–150 m for example) for Bucharest. These values are one of the key input data to algorithms which estimate the spectral acceleration response and transfer functions for every site in which in situ measurements are performed (such as *SHAKE*). As such, in this study we review many recent studies presenting measured V_S values (by different methods) in the Bucharest area and select representative values in order to obtain a homogenized database of mean weighted V_S values at 30, 50, 70 and 100 m. Some values are reprocessed and elevation is extracted from the Digital Elevation Model (DEM) EU-DEM versions 1.1. Maps revealing a broader than previous studies (such as Arion *et al*., 2012, Bălă *et al*., 2010 or Kienzle *et al*., 2006) extent of V_S values are then generated and interpreted.

2. QUATERNARY DEPOSITS IN BUCHAREST CITY AREA

2.1. GENERAL CLASSIFICATION

A first classification on the geological and lithological description of the Quaternary deposits in the Bucharest area is found in Liteanu (1952) and comprise seven main sedimentary complexes (beginning from the surface). The model was considerably improved by Ciugudean-Toma & Ștefănescu (2006), by analysing the probes from several hundreds of boreholes performed in the years 1980’ for the subway of Bucharest. The classification is accepted until today by almost all the scientists involved in the studies of seismic site amplification models and geological modelling, such as Lungu *et al*., (1999), Aldea *et al*., (2006), Mărmureanu *et al*., (2010), Bălă *et al*., (2011), Bălă *et al*., (2013), or Manea *et al*., (2016).

This classification comprises the following names and general characteristics (after Bălă & Hannich 2021):

- **Layer 1: *Anthropogenic backfill and soil***, with a thickness varying between 3–10 m
- **Layer 2: *Upper clayey-sandy complex*** representing Holocene deposits of loess, sandy clays and sands; the thickness of this complex varies between 2 and 5 m in the inter-fluvial domain, 10-16 m in the northern and southern plain and 3–6 m in the river meadows
- **Layer 3: *Colentina gravel complex***, bearing the *Colentina aquifer*, is a layer containing gravels and sands with varying grain size distribution
- **Layer 4: *Intermediate clay layer*** contains up to 80% hard consolidated clay and calcareous concretions with intercalated thin sand and silt lenses; the thickness of this layer varies between 0 and 25 m.
- **Layer 5: *Mostiștea sandbank*,** bearing the *Mostiștea aquifer*, is a sand layer with sands of medium to fine grain size. The thickness varies in the area of Bucharest between 1 and 25 m.
- **Layer 6: *Lacustrine complex*** (or *Lagoon complex*) is composed by a variation of limy-marled clay and fine sands, the grain size < 0,005 mm consisting about 86%.

The thickness varies from about 60 m in the southern part of Bucharest to about 130 m in the North. The variable thickness is due to the underlying *Frățești complex* which descends northward.

– **Layer 7: *Frățești complex***, bearing the *Frățești aquifer*, lies discordant on Pliocene Levantine clay layers. This complex comprises of three thick (10–40 m each) sandy gravel layers (named A, B and C), separated by two marl or clay layers (each of 5–40 m thickness). This thick complex (total thickness 100–180 m), with a continuous presence in the whole area of Bucharest, dips northward; its upper surface lays at about 75 m depth in the southern part of Bucharest and at about 190 m depth in the North.

A more detailed description of the geotechnical characteristics of each layer is given by Ciugudean-Toma & Ștefănescu (2006), which analyse probes from boreholes, presenting the main characteristics of the layers in the depth, in points distributed over the city (figure 1). Mostly due to the characteristics of quaternary deposits in Bucharest, under the influence of seismic waves originating from intermediate-depth Vrancea earthquakes, nonlinear effects have been observed (Cioflan *et al.*, 2009; Mărmureanu *et al.*, 2016) during the 4 March 1977 (moment-magnitude Mw 7.4; 94 km depth), 30 August 1986 (Mw 7.1; 131 km depth) and 30 May 1990 (Mw 6.9; 91 km depth) events (Fig. 1).

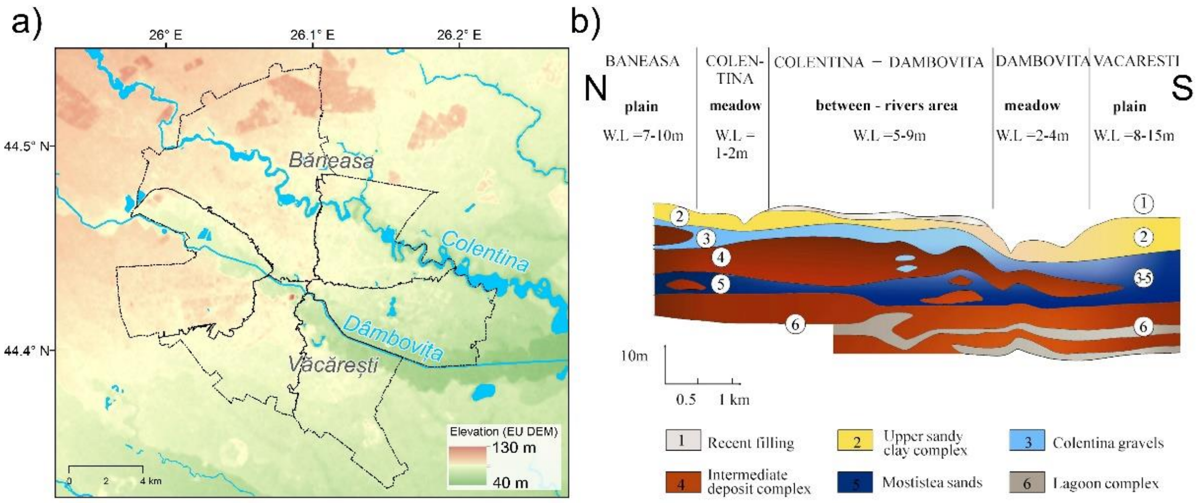

Figure 1 – a) Topographic map of Bucharest (data source: EU-DEM version 1.1.) and b) schematic geomorphologic section (N-S direction), with principal shallow sedimentary layers; depth scale is exaggerated. The section is modified after Ciugudean-Toma & Ștefănescu (2006

2.2. V_S CHARACTERISTICS

For the study of site effects in Bucharest, the necessity to acquire more reliable values of V_S of for Quaternary layers emerged in the years 1997–1999. After these first seismic velocity measurements at INCERC site, other seismic measurements by similar methods and different techniques were performed in Bucharest sites during several Romanian and international research projects.

For standardisation purposes, the Romanian Seismic Design Code (UTCB 2013) recommended that mean weighted values for V_S are computed for each site (borehole) using the following formula:

$$\overline{V}_S = \frac{\sum_{i=1}^{n} h_i}{\sum_{i=1}^{n} \frac{h_i}{V_{Si}}} \tag{1}$$

In equation (1), h_i and V_{Si} denote the thickness (in meters) and the shear-wave velocity (in m/s) of the *i-th* layer, in a total of *n* layers, found in the same type of stratum. According to the same design code, for $\overline{V}_{S30}$, 4 classes of the soil conditions are defined:

– Class A (rock type): $\overline{V}_S$ > 760 m/s
– Class B (hard soil): 360 < $\overline{V}_S$ < 760 m/s
– Class C (intermediate soil): 180 < $\overline{V}_S$ < 360 m/s
– Class D (soft soil): $\overline{V}_S$ < 180 m/s

All the $\overline{V}_{S30}$ values in Table 2 belong to type C of soil after this classification. In Eurocode 8 (European Committee for Standardization, 2004), the values for class A (rock type) are > 800 m/s.

Another critical value in site effects is to estimate characteristic period of the site, defined as period of vibration corresponding to the package of layers from a certain depth to the surface. The vibration period of soil layers in the upper 30 m (T_{S30}) is calculated using Equation 2 in UTCB (2013):

$$T_{S30} = \frac{4h}{\overline{V}_S} \tag{2}$$

where: *h* is ground depth of 30 m.

The characteristic natural period of a specific site (down to a certain depth) has to be considered in relation with vibration period of structure in order to estimate the amplification effects that might occur at the coupling of soft soils/building – resonance. In their study, Aldea *et al*., (2007) considered values of characteristic periods between 0.7–1.53 Hz at 7 sites, according to the depth of the boreholes.

The V_S values obtained by different methods and within several research projects for Bucharest (Bălă *et al*., 2011) were used to determine $\overline{V}_S$ by using equation 1 (columns 3, 5, 7 had to be recomputed from original data). $\overline{V}_S$ values are presented in table 1, for each of the seven Quaternary layers in Bucharest (Table 1).

Table 1

Comparison of $\overline{V}_S$ values [m/s] obtained by different methods for the Quaternary layers in Bucharest between 2002–2009 (modified after Bălă *et al*., 2011)

Number and name of the Quaternary layer	Density [g/cm³]	MOVSP method (7 boreholes) 6 sites	Down-hole method (12 boreholes)	SCPT method (10 sites)	Down-hole method (10 boreholes)	Boreholes measured by UTCB/ NCSRR Down-hole method (7 sites)	Refraction profiles		Mean value and standard deviation
							site A	site B	
1. Backfill	1.75	–	167	–	169	195	140–175	175–195	175.2 m/s ± 8.19 %
2. Upper clay layer	1.96	262	223	262	252	265	275–280	230	253.4 ± 7.99
3. Colentina layer	2.05	340	254	267	320	327	315–350	300–345	308.3 ± 8.19
4. Intermediate Clay layer	2.02	391	319	296	367	364	–	365	350.3 ± 8.19
5. Mostiştea sandbank	2.05	392	350	322	386	405	–	–	371 ± 9.2
6. Lacustrine layer	2.14	429	405	–	417	–	–	–	417 ± 2.8
7. Frăţeşti layer (A)	2.05	511	544	–	–	–	–	–	527.5 ± 4.4

The $\overline{V}_S$ values obtained using different methods such as in boreholes, by penetration tests SCPT or at the surface in Bucharest (seismic refraction) are generally very close. The average densities presented in table 1 are actual densities determined after laboratory measurements in the NATO SfP Project 981882 – the experiment including core sampling of the representative sedimentary layers and determining the geotechnical values for each layer under laboratory conditions (Bălă *et al*., 2011).

Because the shallow Quaternary layers in Bucharest present relative great laterally changes in thickness and also in lithology, the only way to get reliable geotechnical and seismic velocity data may be guaranteed by in situ measurements in boreholes or by special methods on the surface. In order to use the values presented in table 1 for modelling of acceleration response spectra in random points of the Bucharest map, one needs to know the 3D exact position of the seven complexes in the underground of the Bucharest area – a difficult task which shall be completed in the near future with the aid of methods such as Manea *et al*., (2016). For now, the goal in present study is making a database with $\overline{V}_S$ values at standardized depth intervals, as we further present.

3. V_S DATABASE FOR THE BUCHAREST CITY AREA

3.1. DATABASE CHARACTERISTICS

To overcome the problem of heterogeneities of thickness and lithology, providing homogenized input for seismic site amplification models, integrative $\overline{V}_S$ values applicable throughout the whole city area of Bucharest were deduced for four fixed depth intervals (30 m; 50 m; 70 m; 100 m), with no link to the 7 layers earlier presented. V_S values obtained by different methods and authors are used in this database and weighted using equation (1). Final results are organized in a spreadsheet table (available at Toma-Danila *et al*., 2021), which mentions the original data references (shown also in table 2) and also provides interactive mapping, through Microsoft Excel's 3D maps module. Some of the site coordinates had to be redetermined, given the limitations in GNSS determination at the period of the measurement or the decimal degree accuracy and errors in report papers (there are references of modifications in the database) (Table 2).

In table 2 and in the database (Toma-Danila *et al*., 2021) there are:

- 55 points (drillings and SCPT locations) with $\overline{V}_{S30}$ values;
- 48 points for $\overline{V}_{S50}$ values;
- 21 points with $\overline{V}_{S70}$ values;
- 15 sites with $\overline{V}_{S100}$ values.

Values of $\overline{V}_S$ for the 30 m, 50 m depth intervals are between 180 m/s and 360 m/s, so they belong to Class C according to the Romanian Seismic Design Code (UTCB, 2013). For the 70 m and 100 m depth intervals there are a few $\overline{V}_S$ values higher than 360 m/s but without surpassing 390 m/s. In the following subchapters we present the main characteristics of reference data (Figure 2).

Table 2

Drillings and locations used for seismic velocity measurements performed in Bucharest and reported by different authors; all locations are shown on a map in figure 2

No.	Drilling /SCPT-location	Symbol of site	Depth [m]	Method	References
1	INCERC1	INC1	70	CRC 461 Project MOVSP 2002–2003 Multi-Offset Vertical Seismic Profiling (MOVSP)	Orlowsky *et al*., 2003; Hannich & Orlowsky, 2014
2	INCERC2	INC2	100		
3	EREN – AGR	AGR	60		
4	METROUL	MET	100		
5	OPERA – Calea Plevnei	OPE	58		
6	UTCB Tei	UTC	70		
7	Victoriei Square	VIC	150		
8	Grivita	GRIV	110	CERES Project 34, 2002–2003 CERES Project 3–1, 2003–2005	Bălă *et al*., 2005; Bălă *et al*., 2006; Bălă *et al*.,2007; Bălă *et al*., 2009
9	Politehnica	POLT	200		
10	Policolor	POLI	100		
11	Otopeni	OTOP	200		
12	Magurele	MAG	112		

No.	Drilling /SCPT-location	Symbol of site	Depth [m]	Method	References
13	Iorga	IOR	170	Down-hole seismic measurements	
14	Foradex	FORA	81		
15	Buciumeni	BUCU	150		
16	Bazilescu Park	BAZP	172		
17	IMGB	IMGB1	155		
18	Centura 1	CEN1	80		
19	Centura 2	CEN2	60		
20	Tineretului Park	TINE	50	NATO SfP Project 981882 2006–2009 Down-hole seismic measurements	Bălă *et al*., 2007
21	Ecological University	EUNI	50		
22	Astronomic Institute	INAS	51		
23	Titan2 Park	TITAP	50		
24	Motodrom Park	MOTO	51		Ritter *et al*., 2007; Bălă *et al*., 2007; Bălă *et al*., 2008a; Bălă *et al*., 2010
25	Student Park	STUP	50		
26	Bazilescu Park	BAZI1	50		
27	Romanian Shooting Fed.	FRTIR	50		
28	Geology Museum	GEOM	50		
29	National Institute of Earth Physics – Magurele	NIEP	50		
30	Agronomy	AGRO	30	CRC 461 Project Seismic Cone Penetration Test (SCPT) 2003–2005	Hannich *et al*., 2006
31	Bazilescu Park	BAZI2	27		
32	Eroilor	EROI	31		
33	INCERC Institute	INCERC	30		
34	IMGB	IMGB2	22		
35	Meteorological Institute	INMH	32		
36	METRO	METRO	37		
37	Mogosoaia	MOGO	32		
38	Tineretului Park	TINE	27		
39	Victory Square	VICT	33		
40	Basarab Bridge	BAS	30	Down-hole measurements	Lungu & Călărașu 2005
41	A1 Tineretului Park	TINA1	70–90	Seismic refraction lines	vonSteht *et al*., 2008
42	A2 Tineretului Park	TINA2	70–90		
43	A3 Tineretului Park	TINA3	70–90		
44	B4 Bazilescu Park	BAZP4	60–80		
45	B5 Bazilescu Park	BAZP5	60–80		
46	UTCB – Tei	UTC1	78	NCSRR-JICA 2003–2005 Down-hole seismic measurements	Aldea *et al*., 2006; UTCB Report Project 31–038/2007–2008
47	UTCB – Pache Protopopescu	UTC2	66		
48	NCSRR/INCERC	INC	140		
49	Civil Protection	PRC	68		
50	Victoriei Square	VIC	110		
51	City Hall PRI	PRI	52		
52	Municipal Hospital	SMU	69		
53	UTCB – Plevnei	UTC3	30		
54	Sos. Straulesti	SSA	50	Down-hole seismic measurements performed by the research group from UTCB	
55	Romexpo1	EXP1	51		
56	Sos. Fabrica de Glucoza	FGA	50		
57	Obor	OBO	50		
58	Baneasa Forrest	BAN	51		
59	Timpuri Noi	TNO	52		
60	Sos. Floreasca	FLO	50		
61	Romexpo2	EXP2	50		
62	National Park	PNA	50		

No.	Drilling /SCPT-location	Symbol of site	Depth [m]	Method	References
63	Titan 2 Park	PTI2	51		
64	Calea Victoriei	VIC2	52		
65	Sos. Nordului	NOR	50		

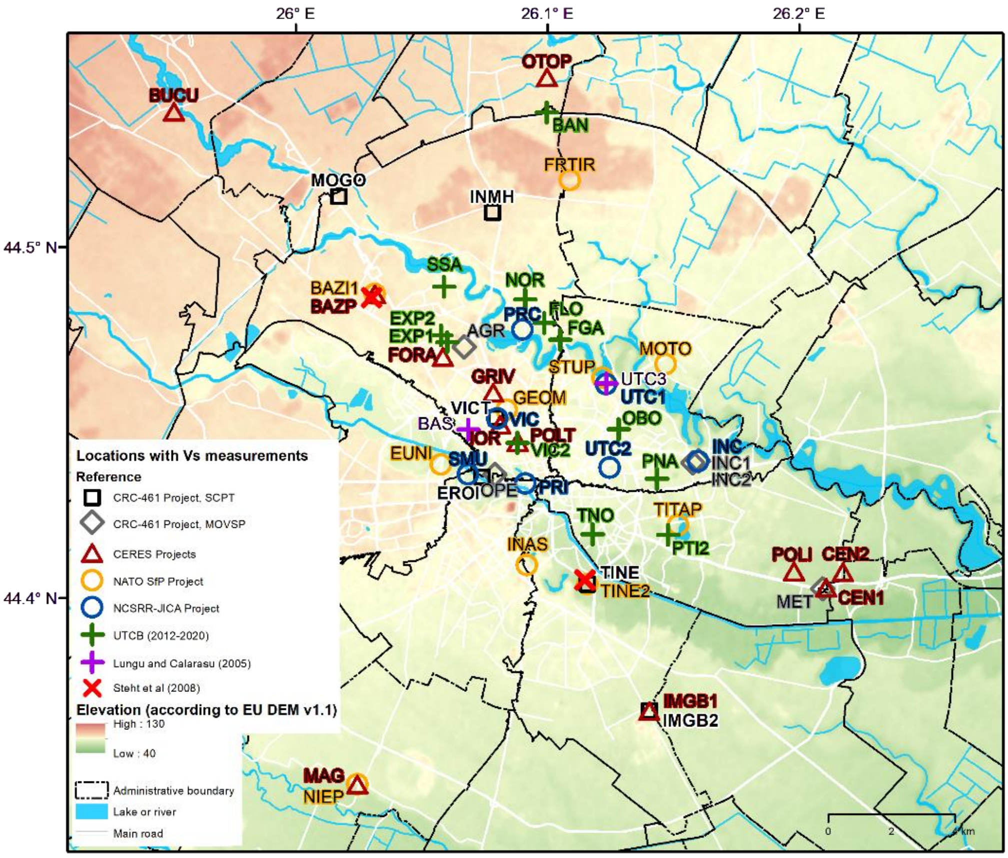

Figure 2 – Map with area under investigation and measurement sites of the different projects and measurement campaigns. The metropolitan region of Bucharest, is mainly inside the characteristic ring road with a diameter of about 20–21 km. The sites with drilling, where seismic and SCPT measurements were done, as indicated by different signs. The red crosses represent the 2 sites where seismic refraction lines were performed.

3.2. CLASSIC DOWN-HOLE MEASUREMENTS REPORTED AT THE END OF 1990'S

In situ measuring and gathering of geotechnical and geophysical data is reported in the late 1990's. Some drillings are reported near the Building Research Institute (INCERC) and some lithological columns appear related to two boreholes: FM3-113 near INCERC (drilling was made before 1989 down to 73 m) and F536 at EREN (74 m). Both are reported in Lungu *et al*., (1997).

In order to find the dynamic properties of the INCERC soil profile, which was considered as a test site, two boreholes were drilled and measured by Institute for Geotechnical and Geophysical Studies (GEOTEC S.A.): INCERC 1 and INCERC 2, in the frame of joint research program CRC 461. For INCERC 2 are presented both the lithological column and the corresponding Vs values down to 77 m depth (Lungu *et al*., 1997). A later borehole (INCERC 3) was drilled in 1998, down to 203 m depth, in order to be instrumented with a borehole accelerometer. In this borehole, a thorough downhole geotechnical measurement was performed by ATLAS-GIP S.A. down to 200 m depth (for layers 4–7), especially for averaged densities of the main geologic layers (Hannich *et al*., 2014).

It is worth to note that 15 specimens extracted from borehole INCERC 2 were from the soil layers 4 and 6, and they were measured in laboratory in order to determine the shear strain modulus ratio G/G_0 versus shear strain as well as the variation of the damping ratio D with shear strain. They were appropriate for low and respectively medium shear strains (Lungu *et al*., 1999).

3.3. MULTI-OFFSET VERTICAL SEISMIC PROFILING (MOVSP) PERFORMED WITH THE COLLABORATIVE RESEARCH CENTRE (CRC) 461 OF KARLSRUHE UNIVERSITY

The MOVSP method is a version of the classic Vertical Seismic Profiling method (VSP). It is called also *Walkaway-VSP* method, because the seismic signals are produced at a lot of source-locations situated along profiles around the borehole. The seismic receivers (geophones) are installed inside the borehole at different depths. In Bucharest, the seismic signals were produced at the surface by a mobile seismic vibrator. The boreholes used for measurements were all equipped with plastic casing to eliminate possible column waves of high velocity as those through steel casing – overlaying the expected useful signals. As well, the boreholes were filled for the measurements with water, because hydrophones are used as seismic receivers, which are installed along a cable-chain hanged in the centre of the borehole (Bălă *et al*., 2011). The MOVSP measurements in Bucharest were carried out in May 2002 and the method and results were published by Orlowski *et al*., (2003). The results of the measurements for each borehole are presented and discussed in Hannich *et al*., (2014). The main disadvantage of this method is that the upper part of the borehole could not be filled with water, due to the local hydraulic conditions of the geologic underground. Thus, for the uppermost 30–35 m depth intervals, respectively for the first three upper Quaternary layers, the seismic velocities could not be obtained. For four sites we have used the values determined later by SCPT method in the same sites, so that we have a complete profile with V_S values (INC1, INC2, EREN, METRO, AGR).

3.4. DOWN-HOLE SEISMIC MEASUREMENTS WITHIN A NATO SFP PROJECT

In the frame of the NATO SfP Project 981882, 10 drillings (20–29 sites in table 2), accompanied by seismic measurements, were performed in 2006–2008 (Bălă *et al*., 2010). The operation was completed by almost continuously core sampling while drilling, leading to the determination of geotechnical properties from each geologic layer after laboratory measurements. Following the completion of the drillings, seismic velocity measurements of V_P and V_S by the classic down-hole method were executed.

Because the depth of the boreholes was limited to 50 m, the deepest Quaternary layer (Frătești layer) was not intercepted. V_S values were recorded from surface down to layers 5 or 6, in all of the ten boreholes, at every meter.

The average densities presented in table 2 are actual densities recorded according to Ciugudean *et al*., (2006), after measurements of several hundred of cores from boreholes of Metroul S.A. laboratory measurements in the frame of NATO SfP Project 981882 – the single experiment used yet to determine geotechnical values (including density) for each layer under laboratory conditions (Bălă *et al*., 2007).

3.5. SEISMIC CONE PENETRATION TESTS (SCPT) PERFORMED IN 2005–2006

To improve the results of the measured V_S for the upper 30–35 m, SCPT were performed within CRC 461, at 10 sites in Bucharest, in 2005–2006 (30–39 sites in table 2). These measurements enabled to obtain new dynamic characteristics for the penetrated geologic layers in the upper 30–32 m and particularly for two shallow aquifers existing in this depth interval. V_S of the corresponding sandy layers under fully saturated, partially saturated and practically dry conditions were obtained – showing quite different values (Hannich *et al*., 2006).

SCPT uses in addition to the conventional CPT-system a seismic acquisition system consisting by three main components: a seismic wave source (hammer-and-beam source for S-waves), a seismic (piezo) cone penetrometer and a recording unit as a PC-based acquisition software. Travel times of body waves propagating between the wave source on the ground surface and an array of geophones in the cone penetrometer are measured. In this way, combined high resolution standard CPT results and seismic wave velocities are presented in parallel, permitting a good correlation of seismic profiling data with stratigraphical, lithological and geotechnical parameters (Hannich *et al.*, 2006).

The results of the SCPT measurements were used first of all for a detailed geological and geotechnical description of the penetrated soil layers. In addition, for the sandy and gravelly layers, variations of the share-wave velocity can be correlated with fully saturated, partially saturated and dry parts of these layers. Finally, based on the standard CPT's pertinent evaluations of the liquefaction potential, the probability of liquefaction and of the safety index of liquefaction in Bucharest by empirical relations was deduced (Bălă & Hannich 2021).

3.6. SITES MEASURED DURING THE NCSRR-JICA COOPERATION IN 2003–2006 AND LATER BY UTCB

Digital seismic equipment donated by the Japan International Cooperation Agency (JICA) to the National Center for Seismic Risk Reduction (NCSRR, Romania) allowed the development of a mixt seismic network in Bucharest, beginning with 2003. In 2005–2006, the network administered by NCSRR contained three types of instrumentation: (i) free-field stations – outside the capital city Bucharest (8 accelerometers); (ii) instrumented buildings - in Bucharest (5 buildings); (iii) stations with free-field and borehole sensors – in Bucharest: 7 sites with ground surface sensor and sensors in boreholes – sites 46–53 in table 2 (after Aldea *et al.*, 2006; Aldea *et al.*, 2007). The boreholes in which the seismic sensors were placed were previously measured by classic down-hole measurement and the results are presented in table 2. From 2003, the down-hole PS logging measurements have been carried out in Bucharest sites in cooperation by UTCB and NCSRR.

Down-hole PS logging have been used as simple and non-invasive geophysical technique for measuring seismic waves velocities, with a depth investigation ranging from 30 m up to more than 140 m. The impulse source of energy is generated at the ground surface, shear wave records being obtained by striking a wood plank horizontally and in opposite direction, while compression wave by dropping a wood hammer on the ground. The velocity sensor is composed by three geophones (2 horizontal and 1 vertical). During down-hole measurements, the sensor was lowered in borehole up to a predetermined depth investigation, being blocked on boring wall for detecting the waves generated by the surface source at 1m depth interval. The equipment system used for velocity measurements was composed of GEODAS acquisition station and PS Logging sensor.

V_S are usually measured by down hole measurements, but later, new methods such as MASW method were employed to obtain V_S values in the first 20 m from surface, at UTCB – Tei site (Arion *et al.*, 2012). Seismic measurements performed by the research group from UTCB were performed in the years 2011–2018 employing down-hole measurements in boreholes down to 50–52 m depth for different local applications. These measurements are included in the database (54–65 sites in table 2).

3.7. V_S DERIVED WITH SASW AND MASW

The seismic velocity is usually measured by down hole measurements, but later some new methods as MASW method are employed to obtain V_S values in the first 25–30 m from surface. The surface waves method is a passive seismic exploration method in which the dispersion character of the surface-waves is analysed and V_S can be obtained only in the first 25–30 m depth. The surface-wave method can be used successfully in the environment of a big city, without the need of drilling a borehole, which makes the method a comparatively cheap one.

Arion *et al.*, (2012) applied the SASW method near the site at UTCB – Tei and presented the results. However, the example presented of a MASW measurement at UTCB site showed V_S between 150 m/s at surface and 210 m/s (at 20 m depth). These are rather low values compared with $V_{S\text{-}30m}$ = 309 m/s, determined for the same site from previous classic down-hole seismic measurements (Aldea *et al*., 2006).

For 7 sites where ground survey was conducted by both down-hole (Arion *et al*., 2012) and MASW methods, a comparative analysis of V_S values corresponding to each depth interval in soil profile has been performed by Călărașu *et al*., (2018). V_{S30} data obtained from MASW are ranging from 189 m/s to 302 m/s, while the values obtained by down-hole are in the range 263–309 m/s. The differences percentages of 15–35% are probably due to constrains of depth investigation limitation, sensors sensitivity, procedure and equipment specificity and lateral discontinuities of soil profile. From both examples presented here we have chosen the values obtained by down-hole to be included in our database.

3.8. OTHER METHODS OF DERIVING V_{S30} AT GLOBAL OR REGIONAL SCALE

Wald & Allen (2007) proposed a methodology that correlates topographic slope data from 30 arc-sec topographic data (recorded by the Shuttle Radar Topography Mission – SRTM30) and V_{S30} values obtained from different sites in USA and several other countries. The results were extrapolated and used to create a global map for V_{S30} values, being available on the USGS server (at https://earthquake.usgs.gov/data/vs30/). However, after farther testing in Europe and Middle East (Wald & Allen, 2007), the recommendation was for the method to be applied with caution for local or site-specific first order studies.

Neagu *et al*., (2018) made a selection of 19 sites in Bucharest in which previously measurements for seismic velocities were performed by PS logging. They found that the difference between seismic borehole measured values and topographical slope estimated values of $\overline{V}_{S30}$ may vary between –23% and +28% for Bucharest. These errors are considerably larger than the computed errors determined in table 2, of about 8–10%. Considering the range of topographical slope estimated values determined for Bucharest, we consider that the results of V_S are not reliable enough for entering in the database for the determination of local seismic hazard in Bucharest, because they will introduce a great amount of uncertainty in the research results.

3.9. PREVIOUS DETERMINATION OF MEAN WEIGHTED V_S

$\overline{V}_S$ values appear in the studies about Bucharest microzonation after 2000. Some $\overline{V}_{S30}$ and $\overline{V}_{S60}$ values are cited in Lungu & Călărașu (2005) – from which we use the record from Basarab bridge (table 2). Bălă *et al*., (2006) have added 3 new values for Politehnica, Policolor and Otopeni.

Aldea *et al*., (2007) provided mean weighted velocities ($\overline{V}_{S30}$ and $\overline{V}_{S52}$), as well as for the whole depth of each borehole which belong to the group of 7 sites which was geophysically examined prior to installation of accelerometers in boreholes.

$\overline{V}_S$ occurred in other studies about Bucharest sites for example in Bălă *et al*., (2008) and Bălă *et al*., (2009a; 2009b). In the second study, a list of 38 sites and 28 sites was used to construct maps for $\overline{V}_{S30}$ and $\overline{V}_{S50}$.

4. MAPS OF THE AVERAGE WEIGHTED V_S

Before mapping the database $\overline{V}_S$ values, data adjustments had to be performed. Different measurement campaigns took place in sites which have been previously used in other campaigns; due to poor descriptions and not precise determination of measurement points, this complicates the identification of some sites and potential duplication. From table 2 we have used some SCPT measurements (no. 30, 31, 33, 36) to complete the previous MOVSP measurements in places where they overlap. In other sites there were also several measurements performed in the same boreholes; for the INCERC test site (Figure 2) we have considered only the last performed measurements presented by Aldea *et al*., (2006) – INC site and the 2 measurements presented by Hannich *et al*.,

(2014) – INCERC1 and INCERC2 sites. Also, 2 sites with MOVSP measurements (UTCB and Victoriei Square) were excluded from the computation, because the values from later measurements in the same sites were preferable.

Sites 41–45 in table 2 represent short refraction lines (up to 300 m), located in 2 parks in Bucharest: Tineretului park (3 lines) and Bazilescu park (2 lines). They are documented in vonSteht *et al*., (2008). However, the velocity values for these sites were not considered for our $\overline{V}_S$ maps, given the method limitations and multiple values per profiles, but only for validation and discussions.

Database values were used to generate (through interpolation), maps of $\overline{V}_S$ at 4 depth intervals, from the surface: 30 m, 50 m, 70 m and 100 m (Figure 3 and Figure 4).

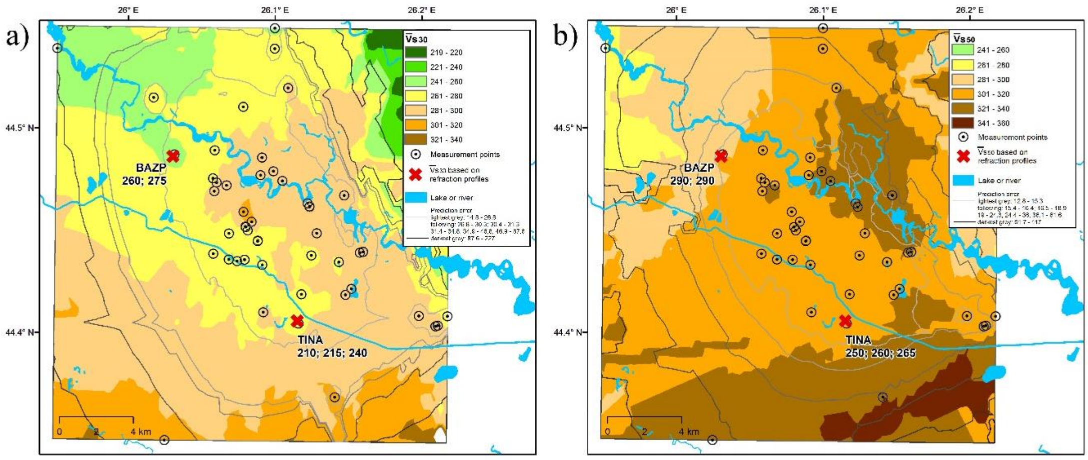

Figure 3 – Maps showing the result of Kriging interpolation of the $\overline{V}_S$ values at some of the sites considered in figure 2 for Bucharest, considering 2 depth intervals: a) 30 m; b) 50 m.

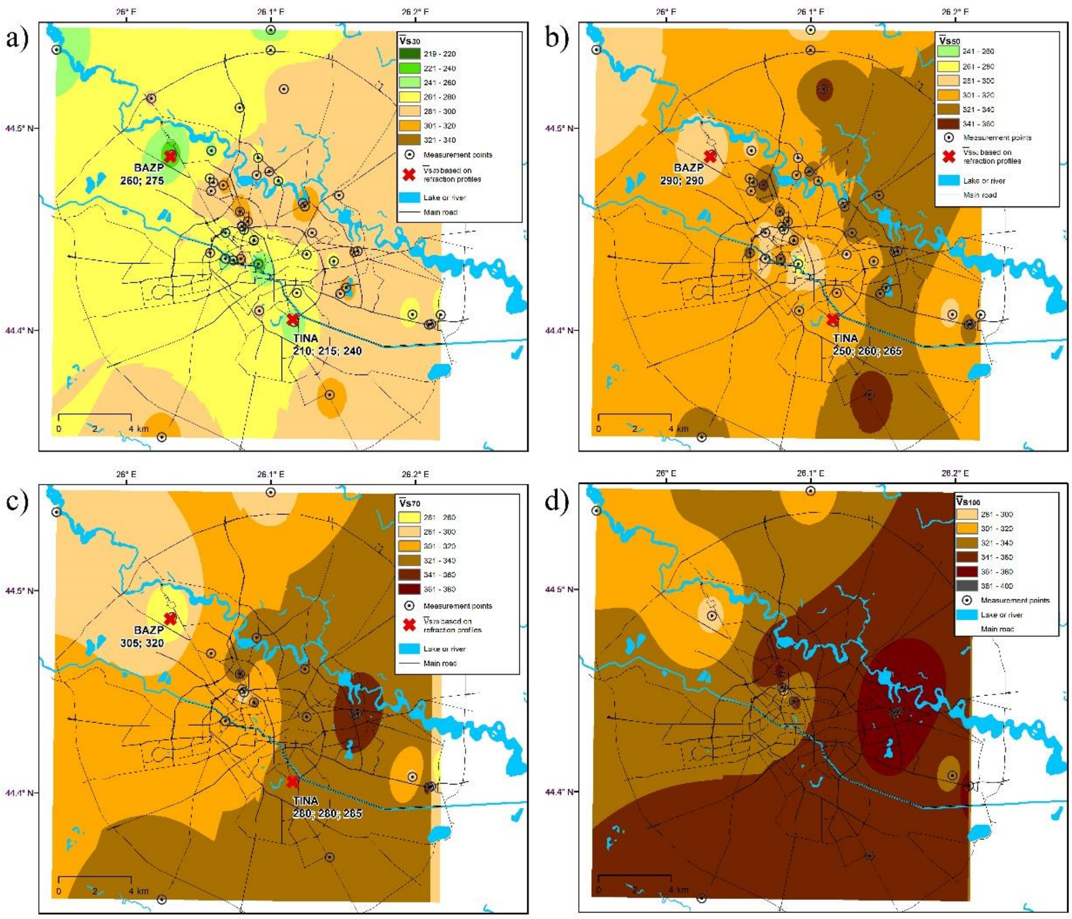

Figure 4 – Maps showing the result of IDW interpolation of the $\overline{V}_S$ values at some of the sites considered in figure 2 for Bucharest, considering 4 depth intervals: a) 30 m; b) 50 m; c) 70 m; d) 100 m.

In order to show an estimate of the expected $\overline{V}_S$ distribution throughout the city, two different sets of maps were created, based on our database, by using two different interpolation methods often used in geophysics (Sun and Kim 2017; Ghazi *et al*., 2014):

1. The kriging method of universal type (figure 3). For this, the parameters chose after multiple testing (due to a better fit of the model to the semivariogram) were Local Polynomial Interpolation of power 1 for trend removal, an account of anisotropy and eight search sectors.

2. The Inverse-Distance Weight (IDW) interpolation method (Figure 4). For this, we used a 12-point influence.

The degree of complexity of each method is different, but in conjunction they can show if a trend maintains or not. IDW assumes that each input point has a local influence that diminishes with distance and is able to keep values of observation in the specific points (but not exceed the minimum and maximum input values); however, it cannot reflect the errors in prediction. This is on the other side the benefit of the more advanced kriging method, used here only for $\overline{V}_{S30}$ and $\overline{V}_{S50}$ due to the fact that for these the number of input values was more satisfactory. Prediction errors are depicted in figure 3 with grey lines; their intervals were chose using the mean geometric classification method. It is to be noted however that kriging modifies the values around the input data, based on the computed statistics relying on a semi-variogram. Both IDW and kriging interpolation was performed using ESRI ArcMap version 10.6 with the geostatistical and spatial analyst toolboxes.

5. DISCUSSION

5.1. V_S MAP INTERPRETATION

The observation that the *SHAKE* types algorithms can provide a better fit between the predicted models of the spectral acceleration response and real recordings at surface if the depth of models is placed at deeper interfaces (Bălă *et al*., 2014) leads to the need for deeper models of the V_S structure in the Bucharest area.

For $\overline{V}_{S30}$ and $\overline{V}_{S50}$, figure 3 and figure 4 show that in the north-eastern part of the city there is an increase in the values; although expected, it seems that the presence of the Pipera swamp as well as the Colentina River does not influence this feature. Across the Dâmbovița River, on both sides, the values are minimum for $\overline{V}_{S30}$, up until the eastern part of the city. $\overline{V}_{S50}$ values appear to be more homogenized for the western and central part of the city. For the south-eastern part of the city, due to the lack of measurement points, the errors can be significant. Especially toward Arges river (10 km south of Bucharest), the V_S values are expected to be smaller in reality.

Most of the measurement sites are concentrated in the centre of the city, in the region that is the Interfluvium between Dâmbovița River and Colentina river. To the north and to the south there are less points, but enough to give a broad image of the V_S characteristics. The sites with low values (220–260 m/s) are concentrated to the north-west, beginning with the first map, while relatively high values are occurring to the west and south parts, if we consider deeper depth down to 70–100 m. Only in figure 4d there are $\overline{V}_S$ values greater than 360 m/s.

The red crosses are marking the two place (Tineretului Park – TIN) and Bazilescu Park – BAZ) in which several refraction lines were performed and the values for the $\overline{V}_S$ on these lines, for the 30 and 50 m depth intervals. Their values are matching the values of the map in the surrounding areas, so they can be considered good checking points for the reliability of the maps.

In the interpretation of the results, some other factors as geomorphological, geological and hydrogeological variations throughout the city need to be taken into consideration. As a trend, figure 4d shows a similar pattern with the topographic map in figure 1; lower $\overline{V}_S$ values correspond to the higher region of the city of 100–130 m altitude, while upper $\overline{V}_S$ values are distributed toward the south-east part, corresponding to lower region of the city (40–80 m altitude).

5.2. THE USE OF V_S IN SPECTRAL ACCELERATION MODELS COMPUTED BY EQUIVALENT LINEAR MODELLING METHOD

Different methods of ground response analysis have been developed including one dimensional, as well as 2D and 3D approaches. Various modelling techniques like the *finite element method* were implemented for linear and non-linear analysis. Extended information on these analyses is given in Kramer (1996). Here we apply an equivalent linear one-dimensional analysis, as implemented in the computer programs for the analysis of geotechnical earthquake engineering problems such SHAKE2000 (Ordonez 2012). The *static soil properties* required in the 1D ground response analysis with SHAKE2000 are: maximum shear wave velocity or maximum shear strength and unit weight. Since the analysis accounts for the non-linear behaviour of the soils using an iterative procedure, *dynamic soil properties* play an important role. The shear modulus reduction curves and damping curves are usually obtained from laboratory test data (cyclical triaxial soil tests). The variation in geotechnical properties of the individual soil layers should be assumed constant for each defined soil layer.

In-built shear modulus reduction curves and damping curves for specific types of layers are used in SHAKE2000 based on worldwide published geotechnical tests (Ordonez 2012). As input data, the interval seismic velocities V_S (in m/s) as well as the natural unit weight (in kN/m^3) and thickness of each layer (in m) were used.

In the research performed in the last years the need for better data acquired by field measurements becomes a necessity and some studies have been made targeting the possibility of acquiring data employing new methods in the field, as well as in the laboratory, where the "field" is in our case a very big and populated city – Bucharest (Bălă *et al*., 2013).

The following input parameters are necessary be introduced in the programs used to compute the spectral amplification, by pseudo-linear site response analysis:

1. The interval seismic velocities V_S (m/s) and mean velocity values weighted with the thickness of each layer will be used for V_S. The shear-wave velocity values will be measured in situ with special designed seismic methods. The thickness of each layer (m) will come from previous selected geologic models as well as the natural unit weight (kN/m3) measured on probes.

2. The shear modulus ratio curves and damping curves versus shear strain (γ) are used in the programs like *SHAKE2000* as built-in curves, although the program permitted the introduction of site-specific curves for a certain location. The engineering procedure requires that the curves will be either determined by measurements applied on the rock samples collected from boreholes drilled in Bucharest City at that time (Lungu *et al*., 1999). They were continued by Arion *et al*., (2006) and Arion *et al*., (2007), who presented the curves of G/G_0 and D/D_o for some samples of clays collected in Bucharest area and measured in laboratory conditions. Later measurements in the area of Bucharest are performed in the frame of NATO Science for Peace Project on samples extracted from principal layers during the digging of the 10 boreholes. The samples were measured in laboratory conditions by the group of UTCB (partners in the project), preserving the humidity of the probes, and the results in the form of G/G_0 and D/D_o were reported by Bălă *et al*., (2013).

3. The strong motion of the ground used as input can be a historic earthquake that has been recorded in the area, in order to reflect the characteristic period would have the arriving strong signal at the site. In theory strong signal should be recorded by a seismometer placed on the bedrock, because the modelling process assumes an input signal traveling from bedrock to surface level.

The engineering bedrock (EB) was proposed in Bucharest area at the upper limit of Frăţeşti A layer first by Lungu *et al*., (1999), for which shear-wave seismic velocities in the domain of 500–550 m/s were reported later by Bălă *et al*., (2007); Bălă *et al*., (2009a); Bălă *et al*., (2009b). One can observe that the proposed interface does not comply with any of the geotechnical requirements which are usually imposed for EB. In Eurocode 8 the shear-wave seismic velocities for the highest grade, type **A** soil, is fixed at 800 m/s, so the bedrock should have a higher velocity, usually by a jump in the values at EB interface.

Other researchers (Cioflan 2006) have documented the existence of EB at the upper limit of rocks with V_S = 1220–1600 m/s, while in the upper part should be rocks with at least 650 m/s. That means for Bucharest the interface between 500–1000 m depth, the boundary which separate the Cretaceous (V_S = 1200–1350 m/s) from Tertiary rocks (V_S = 600–650 m/s), see Bălă (2014).

In theory the interface that is considered the geophysical bedrock should be continuous, composed from a compact rock and extended horizontally under the area of interest: Bucharest city and surroundings. In fact, the local geological situation is much complex.

The Frăţeşti complex is composed of 3 principal layers of gravel which contains important aquifers, separated by layers of compact shale, which have obvious different thickness and heterogeneous characteristics depending on the site.

The upper interface of Frăţeşti layers is dipping from south to north, from 100 m depth at Măgurele (south-west of Bucharest) to about 200 m in Otopeni (north of Bucharest). So, the interface is not horizontal as it is assumed for the EB, but it has a certain gradient, dipping from 90–100 m depth in the south, to 150–160 m depth in the northern part of Bucharest.

After all these observations, supported by recent studies, it can be concluded that the EB cannot be fixed in the underground of Bucharest, since there is no layer having such characteristics, at least in the first 200–300 m depth of sedimentary package. Any layer that is introduced in the modelling as EB and where the strong motion is applied during modelling process should be considered with much care (Bălă 2014).

The average values of shear-wave velocities presented above in table 1 are generally very close, although they were measured by quite different seismic methods in boreholes, by penetration tests (SCPT), or at the surface in Bucharest (seismic refraction). The narrow range in which the mean shear-wave velocities for each of the geologic layer are placed, allows us to use them for the evaluation of mean values for each of the 7 Quaternary layers.

The average densities presented in table 1 are actual densities recorded after laboratory measurements in the NATO SfP Project 981882, the experiment including core sampling of the representative sedimentary layers and determining the geotechnical values for each layer under laboratory conditions Bălă *et al*., (2011).

7. CONCLUSIONS

In the present paper we gather and reinterpret in a new and necessary database V_S values measured through different methods, for Bucharest, the seismically endangered capital of Romania. All measurements are checked with the original sources and $\overline{V}_S$ values are recomputed in some cases, in order to homogenize results. $\overline{V}_S$ values are deduced for 4 fixed depth intervals: 30 m, 50 m, 70 m and 100 m and are used to generate relevant maps.

A main advantage of the database is that its V_S values are measured in situ and computed without any influence from subjective interpretation like the geological interpretation of lithological columns or establishing the limits of the 7 main geological complexes, across the city, like it was done until now.

The database provides evidence to support the distribution of seismic velocities in the Bucharest underground, but most importantly enables further modelling of local site amplification, with better reliability across the city. The main advantage of these maps is that one can design a full network of points at surface, in which the models of spectral acceleration peaks from any interface defined in the ground are to be computed. Given that the maps use a compilation of also newer measured points (compared to older versions such as the ones in Kienzle *et al*., 2006, Bălă *et al*., 2008 or Arion *et al*., 2012) and two interpolation methods reflecting however similar patterns, these can be considered the most relevant attempt to map V_S in Bucharest.

The models are designed to be used to continue the efforts towards a comprehensive microzonation of the Bucharest City by means of enhanced response spectra and transfer functions by equivalent linear modelling methods.

Data availability: The shear-wave velocity database for Bucharest can be retrieved from https://data.mendeley.com/datasets/jncnc6fng9 (Toma-Danila *et al*., 2021)

Acknowledgments. The research work presented in this paper is realized in the frame of various research projects conducted by National Institute for Earth Physics during the years 2001–2011. Following the same research directions, the UTCB research group performed measurements in the field with valuable results and published papers during the years 1999–2018. The cooperation with German scientists from several research Institutes in Karlsruhe, Germany, in the frame of *CRC461 programme – Strong earthquakes: A Challenge for Geosciences and Civil Engineers* is considered to be a great benefit for the advance of the science in the directions of seismic hazard and natural risk reduction in Romania applying deterministic methods and geophysical measurements in Bucharest, Romania.

Funding sources: This research was partially supported by from Pre-Quake project (number PN-III-P1-1.1-PD-2019-0969), supported by a grant of the Romanian Ministry of Research, Innovation and Digitalization, CNCS – UEFISCDI, within PNCDI III and by the MULTIRISC NUCLEU Programme of the National Institute for Earth Physics.

REFERENCES

Aldea, A., Yamanaka, H., Negulescu, C., Kashima, T., Radoi, R., Kazama, H. & Călărașu, E., 2006. Extensive seismic instrumentation and geophyiscal investigation for site-response studies in Bucharest, Romania, in *Proceedings of the Third International Symposium on the Effects of Surface geology on Seismic Motion*, Grenoble, France, paper no. 69.

Aldea, A., Poiata, N., Kashima, T., Albota, E. & Demetriu, S., 2007. NCSRR Digital Seismic Network in Romania, in *Proceedings of the International Symposium on Seismic Risk Reduction*, The JICA Technical Cooperation Project in Romania, 143–156.

Arion, C. & Neagu, C., 2006. Laboratory investigation for estimation of seismic response of the ground, in *Proceedings of 1st European Conference on Earthquake Engineering and Seismology*, Geneva, Switzerland, paper no. 519.

Arion, C. & Neagu, C., 2007. Laboratory investigation for estimation of seismic response of the ground, in *Proceedings of the International Symposium on Strong Vrancea Earthquakes and Risk Mitigation*, Bucharest, Romania, 222–225.

Arion, C., Neagu, C., Văcareanu, R. & Călărașu, E., 2012. In Situ Investigation for Microzonation of Bucharest Surface Geology, in *Proceedings of the 15th World Conference on Earthquake Engineering*, Lisbon, Portugal, paper no. 2034.

Bălă, A., Raileanu, V., Zihan, I., Ciugudean, V. & Grecu, B., 2006. Physical and dynamic properties of the shallow sedimentary rocks in the Bucharest Metropolitan Area, *Romanian Reports in Physics*, **58**, 221–250.

Bălă, A., Ritter, J.R.R., Hannich, D., Balan, S.F. & Arion, C., 2007. Local site effects based on in situ measurements in Bucharest City, Romania, in *Proceedings of the International symposium on Seismic Risk Reduction*, Bucharest, Romania, 367–374.

Bălă, A., Balan, S.F., Ritter, J.R.R., Hannich, D., Huber, G. & Rohn, J., 2007. Seismic site effects based on in situ borehole measurements in Bucharest, Romania, in *Proceedings of the International Symposium on Strong Vrancea Earthquake and risk mitigation*, Bucharest, Romania, 190–204.

Bălă, A., Zihan, I., Ciugudean, V., Raileanu, V. & Grecu, B., 2008. Physical and dynamic properties of the Quaternary sedimentary layers in and around Bucharest City, *Romanian Reports in Physics*, **60**, 389–401

Bălă, A., Aldea, A., Hannich, D., Ehret, D. & Raileanu, V., 2009a. Methods to assess the site effects based on in situ measurements in Bucharest City, Romania, *Romanian Reports in Physics*, **1**, 335–346.

Bălă, A., Grecu, B., Ciugudean, V. & Raileanu, V., 2009b. Dynamic properties of the Quaternary sedimentary rocks and their influence on seismic site effects. Case study in Bucharest City, Romania, *Soil Dynamics and Earthquake Engineering*, **29**, 144–154.

Bălă, A., Balan, S.F., Ritter, J.R.R., Rohn, J., Huber, G. & Hannich, D., 2010. *Site-effect analyses for the earthquake-endangered metropolis Bucharest, Romania*, Alexandru Ioan Cuza Univ. Ed., Iasi, Romania.

Bălă, A., Hannich, D., Ritter, J.R.R. & Ciugudean-Toma, V., 2011. Geological and Geophysical Model of the Quaternary Layers based on in situ measurements in Bucharest, Romania, *Romanian Reports in Physics*, **63**, 250–274.

Bălă, A., Arion. C. & Aldea, A., 2013. In situ borehole measurements and laboratory measurements as primary tools for the assessment of the seismic site effects, *Romanian Reports in Physics*, **65**, 285–298.

Bălă, A., 2014. Quantitative modelling of seismic site amplification in an earthquake-endangered capital city: Bucharest, Romania, *Natural Hazards*, **72**, 1429–1445.

Bălă, A. & Hannich, D., 2021. Liquefaction potential analysis in Bucharest City as a result of the ground shaking during strong Vrancea earthquakes, *Athens Journal of Technology and Engineering*, **8**, 113–138.

Călărașu, E.-A., Arion, C. & Neagu, C., 2018. Geo-data modelling an engineering tool as guidelines for estimating near-surface seismic effects, in *Proceedings of the 16th European Conference on Earthquake Engineering*, Thessaloniki, Greece.

Cioflan, C.O., 2006. *Efecte seismice locale*, Alexandru Ioan Cuza Univ. Ed., Iasi, Romania.

Cioflan, C. O., Marmureanu, A. & Marmureanu, G., 2009. Nonlinearity in seismic site effects evaluation, *Romanian Journal of Physics*, **54**, 951–964.

Ciugudean-Toma, V. & Stefanescu, I., 2006. Engineering geology of the Bucharest city area, Romania, *IAEG Conference: Engineering Geology for tomorrow's cities*, Nottingham, United Kingdom, paper no. 235.

European Committee for Standardization, 2004. Eurocode 8 (EN 1998–1): Design of structures for earthquake resistance – Part 1: General rules, seismic actions and rules for buildings.

Ghazi, A., Moghadas, N.H., Sadeghi, H., Ghafoori, M. & Lashkaripour, G.R., 2014. Spatial Variability of Shear Wave Velocity Using Geostatistical Analysis in Mashhad City, NE Iran, *Open Journal of Geology*, **4**, 354–363.

Hannich, D., Huber, G., Ehret, D., Hoetzl, H., Balan, S., Bălă, A., Bretotean, M. & Ciugudean, V., 2006. SCPTU Techniques Used for shallow geologic/hydrogeologic Site Characterization in Bucharest, Romania, in *Proceedings of the 3rd International Symposium on the Effects of Surface Geology on Seismic Motion*, Grenoble, France, paper no. 71.

Hannich, D. & Orlowsky, D., 2014. Shear-wave velocities of the Quaternary layers determined by Multi-Offset Vertical Seismic profiling (MOVSP) in Bucharest, Romania, *Romanian Reports in Physics*, **66**, 1207–1225.

INCDFP, 2021. *Romplus earthquake catalogue*, http://www.infp.ro/index.php?i=romplus

Lăcătușu, R., Anastasiu, N., Popescu, M. & Enciu, P., 2007. Bucharest Municipality GEO-ATLAS. ESTFalia Ed., Bucharest, Romania (in Romanian)

Liteanu, G., 1952. Geology of the city of Bucharest. Technical Studies, Series E, *Hydrogeology*, **1** (in Romanian).

Lungu, D., Cornea, T., Aldea, A., Nedelcu, C. & Zaicenco, A., 1997. *Seismic microzonation of the city of Bucharest, Romania*, Technical Report for the Association Francaise de Genie Paraseismique, 1, 1–91.

Lungu, D., Aldea, A., Moldoveanu T., Ciugudean V., Stefanica M., 1999, Near-surface geology and dynamic properties of soil layers in Bucharest, in *Vrancea Earthquakes: Tectonics, Hazard and Risk Mitigation*, pp. 137–148, ed. Wenzel, F., Lungu, D. & Novak, O., Kluwer Academic Publishers.

Lungu, D. & Călărașu, E., 2005. Some aspects regarding seismic microzonation of the City of Bucharest, in *Proceedings of the International Conference "Earthquake Engineering in the 21st Century"*, Skopje, Macedonia.

Kienzle, A., Hannich, D., Wirth, W., Ehret, D., Rohn, J., Ciugudean, V. & Czurda, K., 2006. A GIS-based study of earthquake hazard as a tool for the microzonation of Bucharest, *Engineering Geology*, **87**, 13–32.

Manea, E., Clotaire, M., Poggi, V., Fäh, D., Radulian, M. & Balan, S., 2016. Improving the shear wave velocity structure beneath Bucharest (Romania) using ambient vibrations, *Geophysical Journal International*, **207**, 848–861.

Manea, E.F., Michel, C., Hobiger, M., Fah, D., Cioflan, C.O & Radulian, M., 2017. Analysis of the seismic wavefield in the Moesian Platform (Bucharest area) for hazard assessment purposes, *Geophysical Journal International*, **210**, 1609–1622.

Mărmureanu, G., Mărmureanu, A., Manea, E.F., Toma-Danila, D., Vlad, M., 2016. Can we use more classic seismic hazard analysis to strong and deep Vrancea earthquakes?, *Romanian Journal of Physics*, **61**, 728–738.

Mărmureanu, G., Cioflan, C.O. & Mărmureanu, A., 2010. *Cercetari privind hazardul seismic local (microzonare) a zonei metropolitan București*, Technopress Ed. (in Romanian), Iasi, Romania.

Neagu, C., Arion, C., Aldea, A., Călărașu, E.-A., Văcăreanu, R. & Pavel, F., 2018. Ground Types for Seismic Design in Romania, in Seismic Hazard and Risk Assessment: Updated Overview with Emphasis on Romania, pp. 157–172, ed. Văcăreanu, R. & Ionescu, C., Springer Nature.

Ordonez, G.A., 2012. *SHAKE2000: A computer program for the 1-D analysis of geotechnical earthquake engineering problems*, GeoMotions LLC, Lacey, Washington, USA.

Orlowski, D., Witte, C. & Loske, B., 2003. *Execution and evaluation of seismic measurements in Bucharest by the Multi-Offset-Vertical-Seismic-Profiling method (MOVSP)*. Internal Report, DMT, Mines & More Division, Essen (in German).

Raileanu, V., Bălă, A., Hauser, F., Prodehl, C. & Fielitz, W., 2005. Crustal properties from S wave and gravity data along a seismic refraction profile in Romania, *Tectonophysics*, **410**, 251–272.

Sebe, O., Forbriger, T., Ritter, J.R.R., 2009. The shear wave velocity underneath Bucharest city, Romania, from the analysis of Love waves, *Geophysical Journal International*, **176**, 965–979.

Sun, C.G. & Kim, H.S., 2017. GIS-based regional assessment of seismic site effects considering the spatial uncertainty of site-specific geotechnical characteristics in coastal and inland urban areas, *Geomatics, Natural Hazards and Risk*, **8**, 1947–1621.

Thitimakorn, T., 2013. Development of a NEHRP site classification map of Chiang Mai city, Thailand, based on shear-wave velocity using the MASW technique, *Journal of Geophysics and Engineering*, **10**, 045007.

Toma-Danila, D., Bălă, A. & Arion, C., 2021. *Shear-wave velocity database for Bucharest*, Mendeley Data, doi: 10.17632/jncnc6fng9, https://data.mendeley.com/datasets/jncnc6fng9

Toma-Danila, D. & Armaș, I., 2017. Insights into the possible seismic damage of residential buildings in Bucharest, Romania, at neighborhood resolution, *Bulletin of Earthquake Engineering*, **15**, 1161–1184.

UTCB, 2013. *Romanian Seismic Design Code P100–1/2013*

vonSteht, M., Jaskolla, B. & Ritter, J.R.R., 2008. Near surface shear wave velocity in Bucharest, Romania, *Natural Hazards and Earth System Science*, **8**, 1299–1307.

Wald, D.J. & Allen, T.I., 2007. Topographic slope as a proxy for seismic site conditions and amplification, *Bulletin of the Seismological Society of America*, **97**, 1379–1395.

Yaghmaei-Sabegh, S. & Rupakhety, R., 2020. A new method of seismic site classification using HVSR curves: A case study of the 12 November 2017 Mw 7.3 Ezgeleh earthquake in Iran, *Engineering Geology*, **270**, paper no. 105574.

Yordkayhun, S., Sujitapan, C. & Chalermyanont, T., 2015. Shear wave velocity mapping of Hat Yai district, southern Thailand: implication for seismic site classification, *Journal of Geophysics and Engineering*, **12**, 57–69.

PRESEISMIC GEOMAGNETIC ANOMALOUS SIGNAL ASSOCIATED WITH MW8.3 CHILE EARTHQUAKE ON SEPTEMBER 16-TH, 2015

DRAGOȘ ARMAND STANICĂ, DUMITRU STANICĂ

"Sabba S. Ștefănescu" Institute of Geodynamics of the Romanian Academy, 19–21 Jean-Louis Calderon St.,020032 Bucharest, Romania

An earthquake of Mw8.3 hit the coastal zone of Coquimbo (Chile) on September 16th 2015, being also intensively felt along the Argentina border. To identify a possible inter-relation between the pre-seismic anomalous behavior of the geomagnetic polarization parameter (BPOL) and the Mw8.3 offshore Coquimbo (Chile) earthquake, generated on September 16th 2015, in this paper, we retrospectively analyzed the geomagnetic data collected in the 07 July – 21 September 2015 interval, via the Internet (www.intermagnet.com), at the Easter Island (IMP) and Pilar (PIL) geomagnetic observatories, placed in Chile and Argentina, respectively. Consequently, the average daily distribution of the polarization parameter (BPOL) and its standard deviation (STDEV) are performed in ULF range (0.001Hz-0083Hz) by using the FFT band-pass filter analysis. Further on, we investigate the singularity of the pre-seismic anomalous interval associated with the Mw8.3 earthquake by using a statistical analysis based on the standardized random variable equation expressed as: BPOL*=(X–Y)/W. The preseismic anomalous signal was identified with 14 days before the onset of the Mw8.3 offshore Coquimbo (Chile) earthquake.

Key words: Mw8.3 Chile earthquake, Bpol geomagnetic parameter, FFT band-pass filter analysis, ULF-preseismic anomalous geomagnetic signal identification.

1. INTRODUCTION

In the last two decades, the long-term real time ground–based geomagnetic observations done in the seismically active Vrancea zone (Stanica, D., and Stanica, D.A., 2009; 2011, Stanica D.A. *et al*., 2018, Stanica D.A. *et al*., 2020), together with supplementary studies regarding the Mw 9.0 Tohoku earthquake generated on March 11, 2011 (Stanica *et al*., 2015), the Mw 8.1 Chiapas earthquake on September 8, 2017 (Stanica and Stanica, 2019), Mw6.4 Coastal earthquake, Albania (Stanica and Stanica 2021) and the Mw.8.2 Alaska earthquake (D. A. Stanica, 2022) have enlarged our knowledge about the inter-relations among the pre-seismic anomalous geomagnetic phenomena and the final stage of the earthquakes' nucleation. Consequently, in this paper, we retrospectively analyzed the geomagnetic data collected in the 07 July – 21 September 2015 interval via the Internet (www.intermagnet.com), from the Easter Island (IMP) and Pilar (PIL) geomagnetic observatories, placed in Chile and Argentina, respectively (Fig. 1), with the aim to identify possible relationships between the pre-seismic anomalous behavior of the geomagnetic polarization parameter (BPOL) and the Mw8.3 earthquake that occurred offshore Coquimbo (Chile) on September 16th, 2015. Finally, the daily average distribution of the polarization parameter BPOL and its standard deviation (STDEV) are performed in ULF range (0.001Hz-0083Hz) by using the FFT band-pass filter analysis. After analyzing the value of the BPOL parameter obtained at both observatories, PIL being taken as reference one, we used a statistical analysis to identify, on September 2, 2015, a pre-seismic geomagnetic signature related to the Mw 8.3 Offshore Coquimbo earthquake, the lead time being 14 days before the impending earthquake (Fig. 1).

Figure 1 – Map of the Southern America with the Mw8.3earthquake placement on the Chile coastal zone (red star) and the geomagnetic observatories placements: IMP – Easter Island (blue sign) and PIL – Pilar (blue circle).

2. METHODOLOGY, DATA COLLECTION, PROCESSING AND ANALYZING

To identify a pre-seismic anomalous geomagnetic signature related to the Mw8.3 earthquake, it is necessary to obtain information about two factors:

a) Polarization parameter (BPOL):

For a given geoelectric structure, the vertical magnetic component (Bz) is a totally secondary field and it is produced essentially by the Bx horizontal magnetic components (orientated to the North) and By (orientated to the East) and, the polarization parameter expressed as:

$$BPOL (f) = Bz (f) /SQRT[Bx^2(f)+By^2(f)], \quad (1)$$

which should be time invariant in non-seismic conditions and it becomes unstable before the onset of the seismic event.

b) Strain effect-related to the pre-seismic geomagnetic signal identification:

Long range effect of strain-related to the pre-seismic geomagnetic signals is given by (Morgunov, Malzev, Tectonophysics 2007) relation:

$$R\ (km) = 10^{0.5M-0.27}, \quad (2)$$

R is epicentral distance and **M** is earthquake magnitude.

For the M8.3 Coquimbo earthquake the range effect of strain is: **R ~ 7586 km**.

In conformity with Relation (2), the strain effect of the Mw8.3 Chiapas earthquake may be felt at the distance **R ≈ 7600 km**, as in this particular case, the distance between IMP and the earthquake epicenter is about **3500 km** and, respectively, **1000 km** for PIL, so that the condition to identify a pre-seismic anomalous signature is fulfilled in both observatories.

DATA PROCCESING AND ANALYSIS

To carry out a pre-seismic anomalous signature associated with the M_W8.3 Chile earthquake**,** the following steps have been used:

a) An FFT band-pass filter analysis carried out in the frequency range 0.001Hz–0.0083Hz has been performed on the BPOL time series, for two successive time windows of 1024 samples, with 60% overlapping, on the entirely series of 1440 data points acquired each day at the both observatories (Fig.2).

The new time series obtained for the observatories (IMP and PIL) are used to calculate the daily average value of BPOL and its standard deviation (STDEV) in the July 06 – September 21, 2015 interval, and the results are presented in Fig.3 and Fig. 4.

b) To assess the singularity of the pre-seismic anomalous signal related to the M_W8.3earthquake, a statistical analysis based on the standardized random variable Equation (3) was performed:

$$BPOL^*=(X–Y)/W, \qquad (3)$$

where:

- X is 5 days running average of BPOL (IMP) – BPOL(PIL) for a particular day;
- Y is 30 days running average of BPOL(IMP) – BPOL(PIL) before a particular day;
- W is 30 days running average of STDEV (IMP) – STDEV(PIL) before a particular day;
- BPOL*(IMP-PIL) time series emphasizes the threshold for anomaly using STDEV.

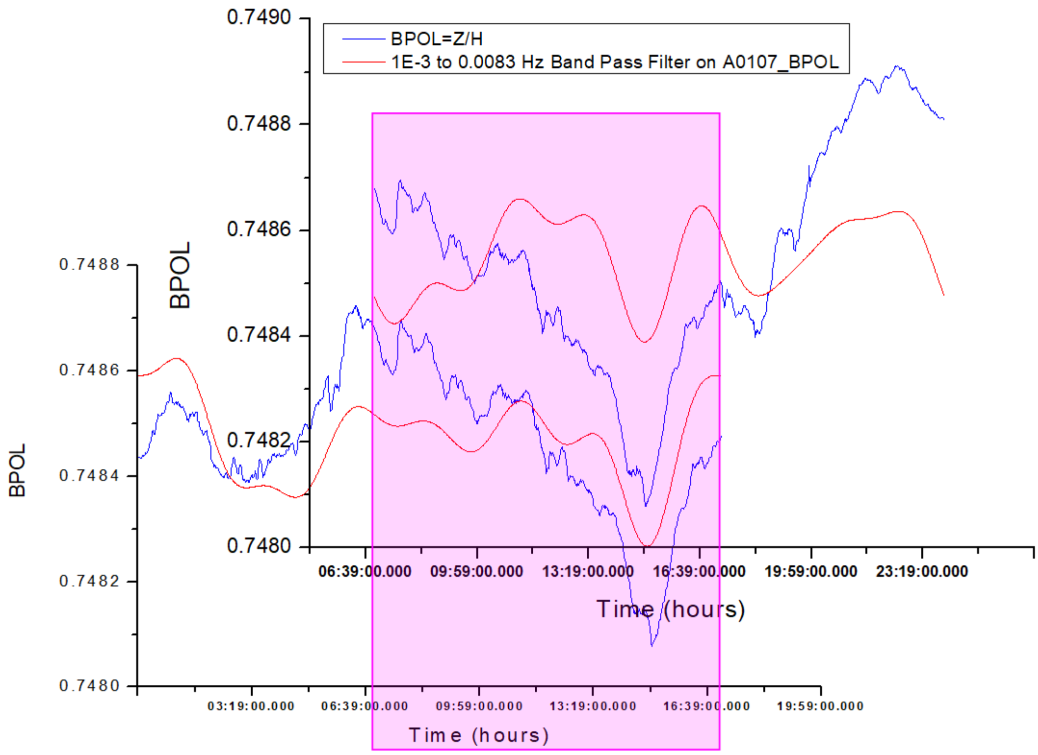

Figure 2 – FFT (Fast Fourier Transform) Band-pass filtering (red line) was applied on BPOL (geomagnetic polarization parameter) time series (blue line) in the frequency range 0.001Hz–0.0083Hz; for a window of 1024 samples carried out using Relation 1.

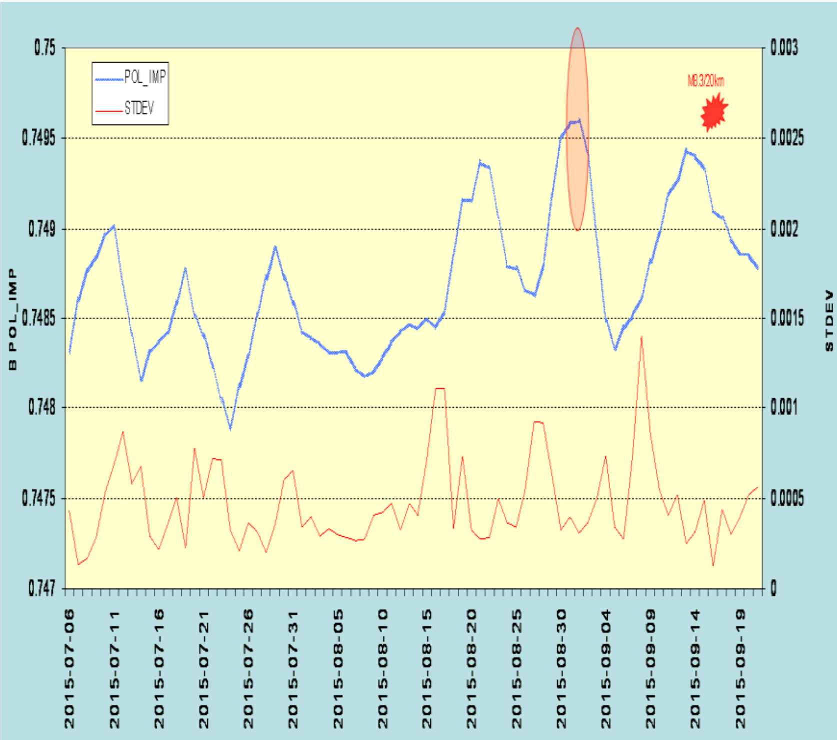

Figure 3 – Daily mean distribution of the BPOL parameter and its STDEV obtained for IMP observatory: red star indicates Mw8.3earthquake, on September 16, 2015; ratio 8.3/20km is magnitude/hypocenter; red ellipse emphasizes the pre-seismic geomagnetic signal.

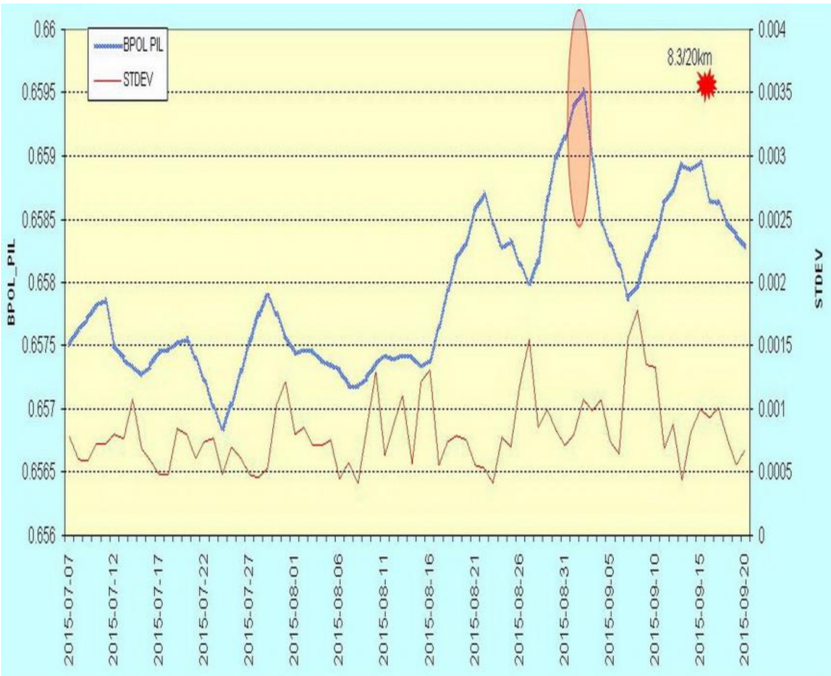

Figure 4 – Daily mean distribution of the BPOL parameter and its STDEV obtained at PIL observatory, red star indicates Mw8.3earthquake, on September 16, 2015; ratio 8.3/20km is magnitude/hypocenter; red ellipse emphasizes the pre-seismic geomagnetic signal.

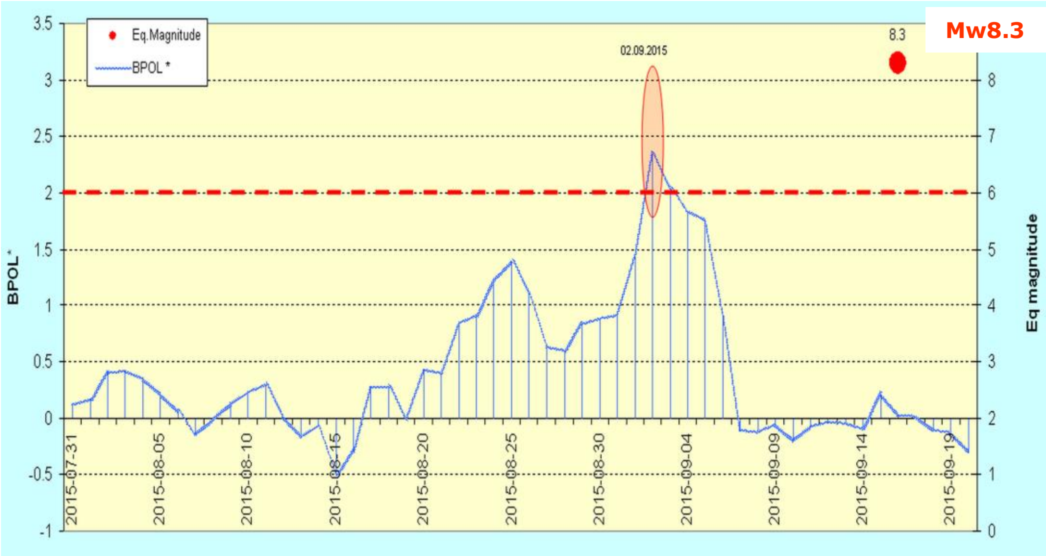

Figure 5 – Daily distribution of the parameter BPOL* on the interval August 1 – September 19, 2015 (blue line). Red full circle is Mw8.3earthquake, red ellipse is a pre-seismic anomalous signature of the Mw8.3 on September 2, 2015, red dashed line represents threshold for anomaly using STDEV.

CONCLUSIONS

In order to emphasize the possible interrelation between the pre-seismic geomagnetic signature and the Mw8.3 Chile earthquake, in this paper we have investigated the ULF geomagnetic data collected in the 06.07–20.09.2015 interval at the Easter Island (IMP) and Pilar (PIL) geomagnetic observatories, placed in Chile and Argentina, respectively. Thus, the daily average distributions of the BPOL(IMP) and BPOL(PIL), presented in Figures 3 and 4, were analyzed for the July–September, 2015 interval, both emphasizing on September 3, 2015 two very high amplitudes of the geomagnetic parameters (BPOL=0.659 for PIL and BPOL = 0749 for IMP), both being associated with the Mw8.3earthquake, suggesting the existence of a co-seismic effect.

The proposed methodology regarding the distribution of the geomagnetic polarization parameters BPOL and BPOL*, last one being obtained by using a standardized random variable equation (relation 3), provides adequate information to identify, starting with September 2, a peak level higher than 2 BPOL* (red dashed line in Fig. 5), the lead time being 14 days before the onset of the M8.3 offshore Coquimbo (Chile) earthquake (read ellipse).

Acknowledgements. The results presented in this paper are based on data collected at Geomagnetic Observatories Easter Island (IMP) and Pilar (PIL) that are placed in Chile and Argentina. We thank the national institutes that support them and the INTERMAGNET for promoting high standards of magnetic observatory practice (www.intermagnet.org).

REFERENCES

Morgunov V.A., Malzev S.A. (2007). A multiple fracture model of pre-seismic electromagnetic phenomena, Tectonophysics 431, 2007, pp. 61–72.

Stanica, D., and Stanica, D.A., 2009. Constraints on correlation between the anomalous behavior of electromagnetic normalized functions (ENF) and the intermediate depth seismic events occurred in Vrancea zone (Romania), Terr. Atmos. Ocean. Sci., vol.21, No. 4, 675–683, August 2010, doi:10.3319/TAO.2009.09.09.01(T).

Stanica D., Stanica D.A. (2011). Anomalous pre-seismic behaviour of the electromagnetic normalized functions related to the intermediate depth earthquakes occurred in Vrancea zone, Romania, Nat. Hazards Earth Syst. Sci., 11, pp. 3151–3156, doi: 10.5194/nhess-11-3151, 2011.

Stanica D.A., Stanica D., Vladimirescu N. (2015). Long-range anomalous electromagnetic effect related to M9 Great Tohoku earthquake. *Earth Science*. Vol.4x, No.1, pp.31–38. 2015, doi:10.11648/j.earth.20150401.13.

Stanica D.A., Stanica D., Blecki J., Ernst T., Jozwiak W., Slominski J. (2018). Pre-seismic geomagnetic and ionosphere signatures related to Mw5.7earthquake occurred in Vrancea zone on September 24, 2016, pp.167–177, https//doi.org/10.1007/s11600-018-0115-4.

Stanica D.A., Stanica D. (2019). ULF Pre-seismic geomagnetic anomalous signal related to Mw8.1 offshore Chiapas earthquake, Mexico on 8 September 2019, Entropy 2019, 21, 29; pp.1–11, https://doi:org/10.3390/e21010029.

Stanica D. A., Stanica D., Valeca M., Iordache S., (2020). Electromagnetic contribution to the resilience improvement against the Vrancea intermediate depth earthquake, Romania. ANNALS of GEOPHYSICS, 63, 5, PA551, 2020: Doi: https://doi.org/10.4401/ag-8096

Stanica D.A., Stanica D. (2021). Possible correlations between the ULF geomagnetic signature and Mw6.4 Coastal earthquake, Albania, on 26 November 2019, Entropy 2021, 23, 233. https://doi.org/10.3390/e2302233.

Stanica D., Stanica D.A. (2021). Pre-seismic geomagnetic anomalous signature related to Mw.7.0 earthquake generated in the northern coastal zone of Samos Island-Greece on October 30, 2020, EGU21-1078, https://doi.org/10.5194/egusphere-egu21-1078.

Stanica D.A. (2022). Anomalous geomagnetic signal emphasized before the Mw8.2Coastal Alaska earthquake, occurred on 29July 202, Entropy 2022,24, 274. https://doi.org/10.3390/e24020274.

SUB-CENTENNIAL VARIATIONS IN THE HORIZONTAL COMPONENT OF THE GEOMAGNETIC FIELD. PRELIMINARY RESULTS

CRISTIANA ȘTEFAN[1], VENERA DOBRICĂ[1], CRIȘAN DEMETRESCU[1,2]

[1]*Institute of Geodynamics, Romanian Academy*
[2]*Academy of Romanian Scientists*

The study is based on H geomagnetic data returned by the long-term model of the main geomagnetic field *gufm1* (Jackson *et al*., 2000) in a grid of 2,5×2.5 degrees of latitude/longitude, for the time interval of the model validity (1590–1990). Each time series returned by the model was first subjected to a Hodrick and Prescott (HP) analysis (1997), to separate a decadal variation from a so-called trend, and then the trend to a Butterworth (1930) filtering, to retrieve inter-decadal (20–30 years time scale) and sub-centennial variations (60–90 years time scale). Characteristics of the latter are discussed pointing to external primary sources (magnetospheric ring current and ionospheric polar current systems).

Key words: geomagnetic field models, multi-decadal oscillations, external current systems.

1. INTRODUCTION

It is common knowledge that in the annual averages of geomagnetic elements provided by geomagnetic observatories there is an external residual variation, not averaged out, that results in an 11-year-solar-cycle variation in H and Z time series of observatory annual means. In Fig.1 we present, as an example, the evolution of the Dst geomagnetic index during the moderate geomagnetic storm of August 22–27, 2005, showing that the depression of the geomagnetic field during the main phase of the storm is not compensated in the annual average by any increase of the field during the recovery phase of that storm. Indeed, Demetrescu and Dobrică (2014) showed the presence of this variation in case of H time series provided by 24 observatories with long activity (100–150 years). They also detected variations at two other time scales, namely ‘inter-decadal’ (20–30 years) and ‘sub-centennial’ (60–90 years) ones, as they were coined later (Ștefan *et al*., 2017, Dobrică *et al*., 2021) and noticed that, not accounting for these variations before modelling the main field using observatory and/or historical data, they appear in the field evolution described by long-term models of the main field, such as *gufm1* (Jackson *et al*, 2000), or COV-OBS (Gillet *et al*., 2013). In Fig. 2 we show the 11-year-solar-cycle variation in observatory and long-term geomagnetic field models data, compared to the solar sunspot number.

2. DATA AND METHOD

In the present paper, we analyze time series of the geomagnetic field returned by the *gufm1* model in a grid of 2.5×2.5 degrees of latitude/longitude of the European continent. Like Dobrica *et al*. (2018), we use the Hodrick and Prescott (1997) type of analysis that separates the cyclic variation at a decadal time scale from the trend in data, followed by a Butterworth filtering (Butterworth, 1930) of the trend to extract the inter-decadal and the sub-centennial variations. We focus here on the sub-centennial variation, as having the largest amplitudes (see further below) and draw some preliminary conclusions on that variation in the geomagnetic field.

Fig. 3 illustrates the above-described filtering procedure used in this paper for a point corresponding to the position of the Niemegk geomagnetic observatory (IAGA code NGK), central to the European network of observatories. The analysis also involved the magnetic declination (not swown), a less studied geomagnetic element (see Stefan *et al.*, 2023).

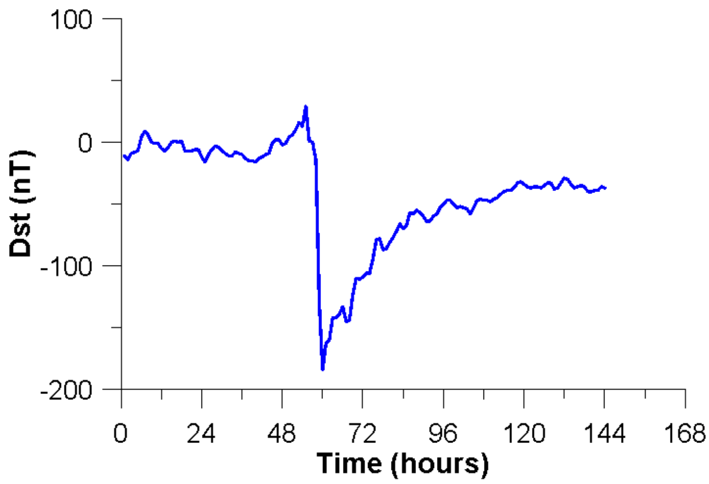

Fig. 1 – The evolution of certain geomagnetic storm, illustrated by means of the Dst geomagnetic index characterizing the moderate storm of August 22–27, 2005.

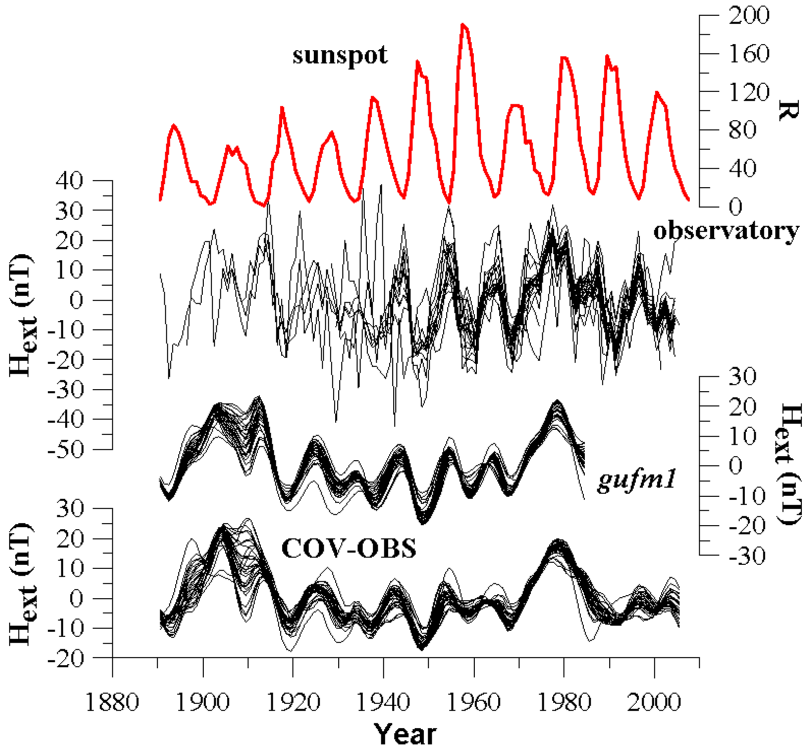

Fig. 2 – Decadal variation in observatory annual means and in long-term main field models *gufm1* and COV-OBS, as compared to the sunspot number time series.

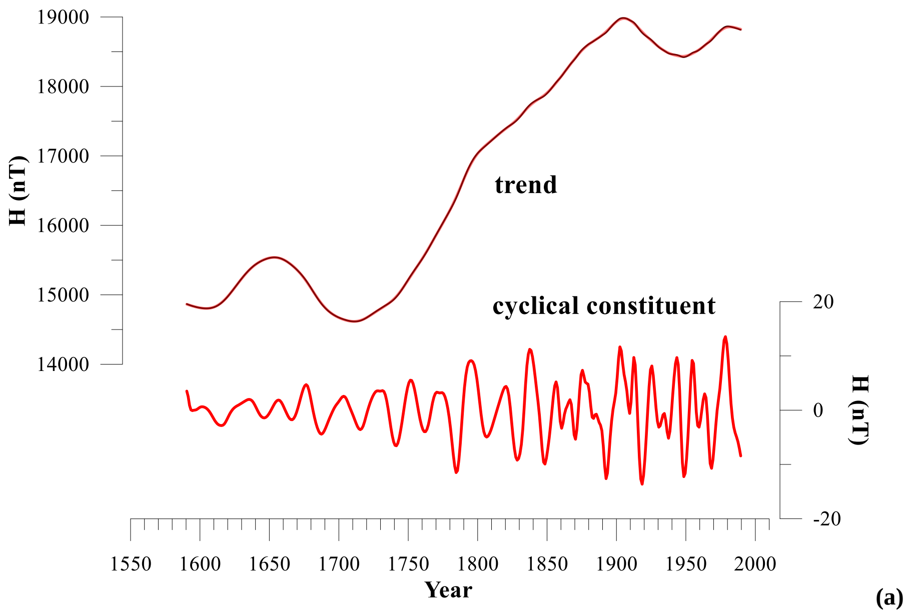

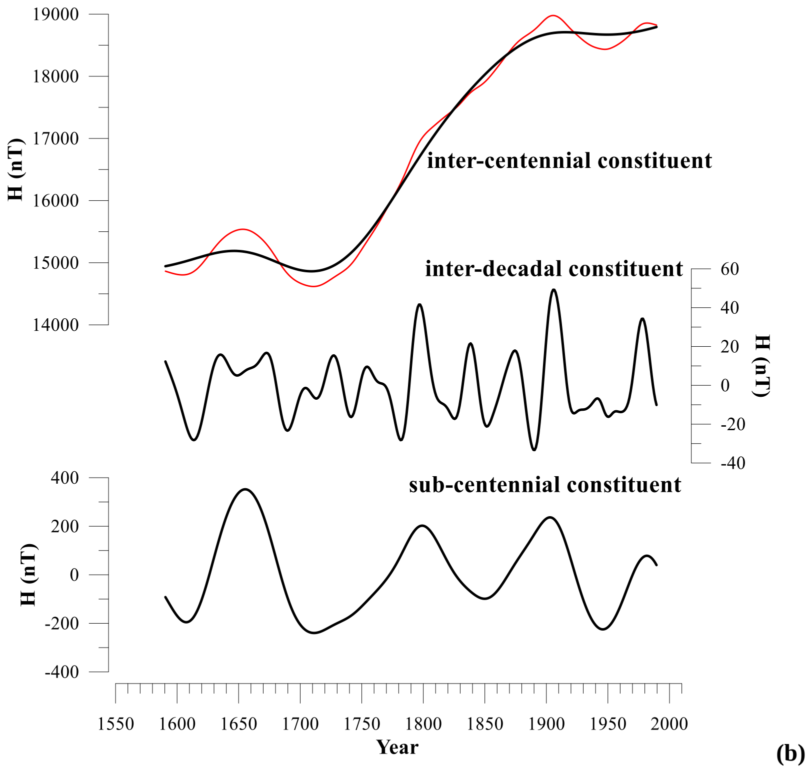

Fig. 3 – Filtering procedure: (a) HP filter; (b) Butterworth filter. Illustration for a point corresponding to Niemegk geomagnetic observatory (IAGA code, NGK).

3. RESULTS AND DISCUSSION

Fig. 4 shows the evolution of the sub-centennial constituent for several latitudes between 40 and 70°N. A few characteristics can be distinguished at this stage, namely the oscillatory character, with amplitudes amounting to 800 nT in case of low – mid-latitude points, much higher than in case of the other swub-centennial variations, namely decadal (cca 30 nT) and inter-decadal (cca 100 nT) ones (see Fig. 3). In case of high-latitude points of the grid (>50°N), several other oscillations appear. This general behavior points to external sources, namely the magnetosphere ring current and, respectively, the polar ionosphere currents that form as a result of the interaction between the solar wind and the magnetosphere. Time-longitude plots (Hovmöller, 1949) of the three oscillatory features (Fig. 5) also point to the same external origin, showing elongated strips of the same amplitude, slightly inclined with respect of the geographical coordinates. They probably reflect induction effects of the mentioned external current systems that are organized by the orientation of the geomagnetic axes; a separate quantitative study is however necessary, having in view their large amplitudes (Demetrescu *et al.*, 2023, in preparation). For the moment, we remind the reader the oscillations seen in the heliosphere-magnetosphere environment by Demetrescu *et al.* (2010) that point to oscillations in the external current systems. Another important conclusion refers to the certain diminishing of period in the recent times, from 130 years in the time span 1620–1750, to 110 years in the time span 1870–1980, illustrating a certain variation in the past of the effectivity of the solar activity.

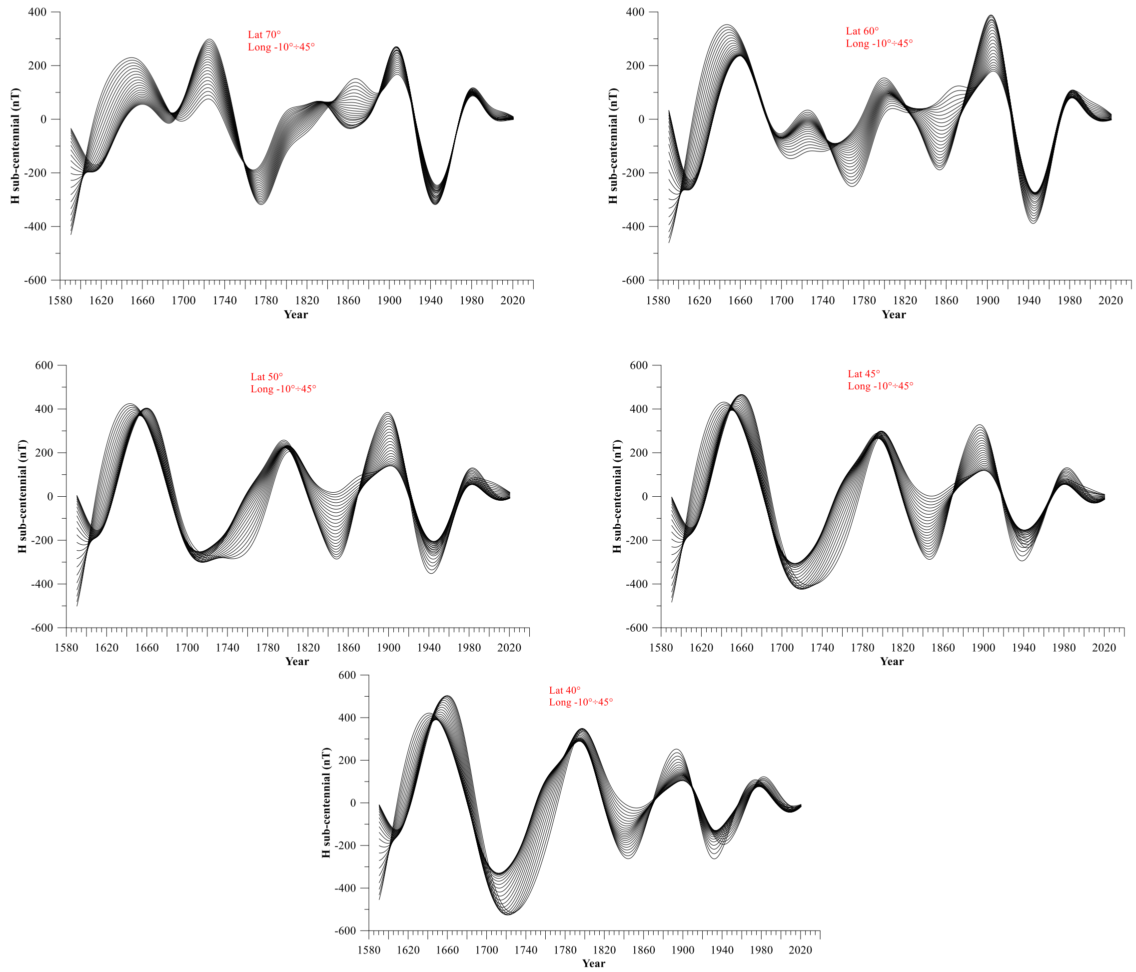

Fig. 4 – The evolution of the sub-centennial constituent for several latitudes between 40° and 70°N.

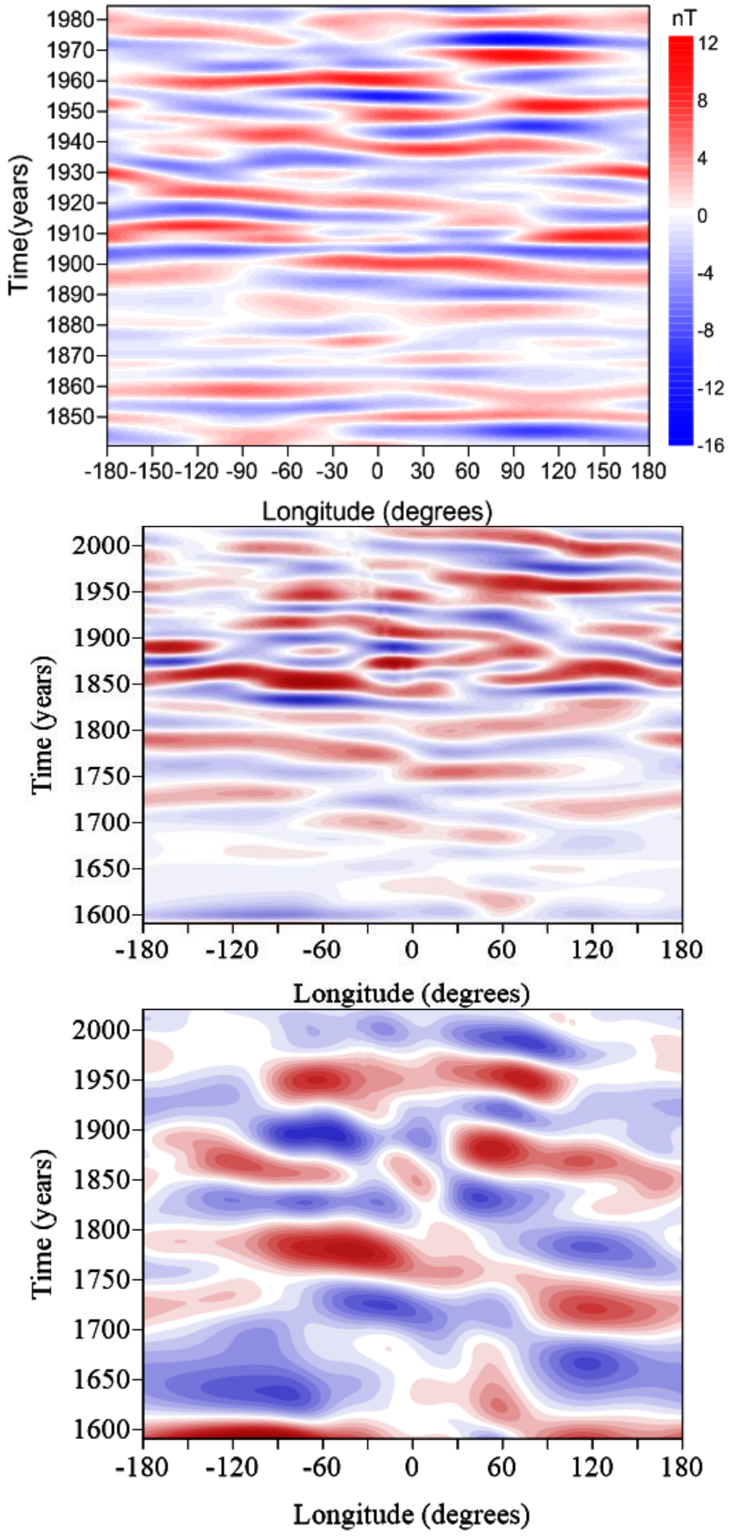

Fig. 5 – Time-longitude plots of the three oscillatory features. From top to bottom: decadal, inter-decadal and sub-centennial.

4. CONCLUDING REMARKS

In this paper have been discussed preliminary results on the sub-centennial variation seen in long-term model *gufm1* of the main geomagnetic field (Jackson *et al*., 2000). This variation has been noticed first in annual mean time series produced by geomagnetic observatories (Demetrescu and Dobrică, 2014).

Among the main conclusions we may emphasize: the oscillatory character, the latitude dependency of these variations, and the past variation of the frequency content. They all point to an external primary origin. Additional work is necessary to disentangle further details, such as the contribution of the induced response of the Earth's interior to the observed variations.

REFERENCES

BUTTERWORTH S. (1930), *On the theory of filter amplifiers*, Wireless Engineer, **7**, 536–541.

DEMETRESCU C., DOBRICĂ V. (2014), *Multi-decadal ingredients of the secular variation of the geomagnetic field. Insights from long time series of observatory data*, Phys. Earth Planet. Inter., **231**, 39–55, https://doi.org/10.1016/j.pepi2014.03.001.

DEMETRESCU C., DOBRICĂ V., MARIȘ G. (2010), *On the long-term variability of the heliosphere–magnetosphere environment*, Adv. Space Res., **46**, 1299–1312, doi: 10.1016/j.asr.2010.06.032.

DEMETRESCU C., DOBRICĂ V., ȘTEFAN C. (2023), *On the drivers of the multi-decadal oscillations in the geomagnetic field,* in preparation.

DOBRICĂ V., DEMETRESCU C., MANDEA M. (2018), *Geomagnetic field declination: from decadal to centennial scales*, Solid Earth, **9**, 491–503, https://doi.org/10.5194/se-9-491-2018.

DOBRICĂ V., ȘTEFAN C., DEMETRESCU C. (2021), *Planetary scale geomagnetic secular variation foci in the last 400 years*, Global and Planetary Change, **199**, 103430, https://doi.org/10.1016/j.gloplacha.2021.103430

HODRICK R.J., PRESCOTT E.C. (1997), *Postwar U. S. business cycles: An empirical investigation*, J. Money, Credit, Banking, **29**, 1–16.

HOVMÖLLER E. (1949), *The Trough-and-Ridge diagram*, Tellus, **1**, 62–66.

JACKSON A., JONKERS A.R.T., WALKER M.R. (2000), *Four centuries of geomagnetic secular variation from historical records*, Phil. Trans. R. Soc. Lond., **358**, 997–990.

ȘTEFAN C., DOBRICĂ V., DEMETRESCU C. (2023), On sub-centennial variations in the geomagnetic declination,, Rev. Roum. Géophys., in preparation.

ȘTEFAN C., DOBRICĂ V., DEMETRESCU C. (2017), *Core surface sub-centennial magnetic flux patches: characteristics and evolution*, Earth Planets and Space, **69**, 146. https://doi. org/10.1186/s40623-017-0732-1.

GILLET N., JAULT D., FINLAY C.C., OLSEN N. (2013), *Stochastic modeling of the Earth's magnetic field: Inversion for covariances over the observatory era*, Geochem. Geophys. Geosyst., **14** (4), 766–786.

UNLOCKING NEW RESOURCES IN COMPLEX TECTONIC SETTINGS AN INSIGHT INTO THE PROSPECTIVITY AND PETROLEUM SYSTEMS OF THE NANKAI ACCRETIONARY PRISM

CĂLIN CONSTANTIN NIȚĂ[1], IZABELA MARIȘ[1], IOAN MUNTEANU[1,2]

[1] *Faculty of Geology and Geophysics, University of Bucharest, Bucharest, Romania*
[2] *„Sabba S. Ștefănescu" Institute of Geodynamics of the Romanian Academy*

Recent advances in seismic acquisition and processing have allowed research centers and corporations all over the world to move the frontiers of hydrocarbon exploration in complex areas, such as subduction zones. Three dimensional seismic surveys, corroborated with log data, tops and biostratigraphic ages from wells, now permit geoscientists to define sedimentological models, and to characterize deformation mechanisms and visualize the extent of various thrust sheets structures in accretionary prisms. The focus of this study is to integrate 672 square km of seismic coverage with data from available wells in order to understand the petroleum systems from the Nankai region. In the final step, we would like to define multiple prospects along with the hydrocarbon products, estimating the recoverable resources that these host.

Key words: seismic, Nankai, gas, subduction, accretionary prism, petroleum systems, exploration.

1. INTRODUCTION

Accretionary prisms represent tectonic edifices that form at convergent plate margins. They are specific fold and thrust belts that grow in response to subduction of the lower plate and accretion of the sedimentary deposits at the upper plate (Beaumont, 1981; Uyeda, 1981). The continuous pursuit for new oil and gas fields marks the abandonment of depleted areas, such as passive margins or continental aulacogens and foreland basins, and the onset of exploration in such challenging compressional environments.

The Nankai accretionary complex is a young Miocene-Quaternary fold and thrust belt formed as a result of the migration of the Boso Triple Junction and the reactivation of the Philippine Sea Plate subduction underneath the Eurasian Plate around 6 Ma ago. It is located in southwest Japan and holds an amazing potential for hydrocarbon resources. In this study, using seismic and well data, we intend to reveal the biogenic gas system in this region and to define a couple of prospects in order to understand if the accretionary complex yields an economic profitability.

2. GEOLOGICAL SETTING

The study area is located along the southwestern margin of Japan, near the Kii Peninsula (Fig. 1). This region is characterized by a convergent tectonic setting which commenced around 6 Ma, when the Philippine Sea Plate subduction beneath the Eurasian Plate was resumed after a pause that lasted for almost 8 Ma (Kimura *et al*., 2014). The Philippine Sea Plate is moving to the north-west, following a 300º–315º azimuth, at a subduction rate of 4 to 6.5 cm per year (Miyazaki and Heki, 2001; Zang *et al*., 2002; Seno *et al*., 2013).

The Nankai system is represented by the accretion of a thick (over 1000 m), mostly terigenous, succession which is made up of the formations deposited in the oceanic trench and in the Shikoku Basin (Park *et al*., 2002), an Oligo-Miocene back-arc basin (Seno and Maruyama, 1984; Chamot-Rooke *et al*., 1987; Hibbard and Karig, 1990) that develops in the northern part of the Philippine Sea Plate (Shiraishi *et al*., 2019), close to the Izu-Bonin island arc (Okino *et al*., 1994). The Shikoku depocentre includes sedimentary deposits that consist mostly of turbidites and hemipelagic muds, along with pelagic shales and tephras in a reduced proportion (Shiraishi *et al*., 2019).

The Nankai fold and thrust belt can be tectonically divided in two major domains (Fig. 2), the inner accretionary prism and the outer accretionary prism, these two being separated by a transition zone which is marked through a major strike-slip megasplay fault, known as the Kumano Basin Edge Fault Zone (KBEFZ) (Kimura *et al*., 2007).

Fig. 1 – Location of the study area within the Japanese Archipelago (Google Earth Pro).

Fig. 2 – Regional TWT seismic cross section along the Nankai accretionary prism showing the main tectonic elements.

The inner prism is a double-vergent accretionary complex that is comprised of highly deformed nappes and the overlying sediments of the Kumano Forearc Basin (Fig. 2). The age of the inner prism thrust sheets varies from 5.9 to 8.1 Ma, in accordance with the ages obtained from the cores that were collected in the Integrated Ocean Drilling Program, indicating that the subduction process was initiated circa 6 Ma (Saffer *et al*., 2009; Gulick *et al*., 2010; Moore *et al*., 2015; Boston *et al*., 2016). The growth of the Kumano Basin triggered a sedimentary loading subsidence mechanism that gradually stabilized the inner prism from a mechanical point of view. This marked the onset of a new compressional cycle which led to the formation of the outer prism, a unit that has been tectonically active in the last couple Ma. Deformation is mainly concentrated in the frontal zone of the fold and thrust belt (Screaton *et al*., 2009; Moore *et al*., 2015). The outer accretionary complex presents an imbricate structure (Fig. 2) that allowed the development of slope basins above the nappes (Strasser *et al*., 2009; Kimura *et al*., 2011).

3. DATASET AND METHODOLOGY

The dataset for this project consisted of a TWT (PSTM) seismic cube that covers almost 672 square km and seven wells (only borehole COOO6 data was used in this study) with the associated geological and geophysical information (tops, logs, cores, reports) (Fig. 3). Another seismic volume, in depth (PSDM), was also available, but it was not selected for interpretation due to the fact that it had a considerably smaller coverage area. The JAMSTEC Agency from Japan acquired and processed the seismic survey in 2006 for scientific research regarding the origin of tsunami generating earthquakes in the region.

Fig. 3 – The dataset that was made available by the JAMSTEC Agency in Japan (seismic) and the IODP Program (wells). In this study we focused on the petroleum systems from the outer prism (red polygon) using the seismic survey and well COOO6. The pseudo-well used for the depth conversion is referenced with the red arrow.

The Kingdom 2017 software was used to manipulate the data in the project. A classic seismic interpretation was carried at a 10 line increment using the principles of seismic sequence stratigraphy. Key surfaces, such as the Bottom Simulating Reflector (BSR) and the tops of the reservoirs, and major thrust faults were mapped in order to understand the geometry and architecture of the thrust sheets in the outer accretionary prism. At the same time, the V_{shale} curve was defined in well COOO6 using the gamma ray log (Fig. 4), with the purpose of creating a depositional model and estimating the lithology variations along the succession (different cut-off values were used to delineate the types of sedimentary rocks: 0–25 for sands/sandstones, 25–35 for silty sands/silty sandstones, 35–55 for silts, 55–60 for silty shales, 60–100 for shales; Fig. 4).

Fig. 4 – V_{sh} curve obtained by processing the gamma ray log (A) and the associated lithology that was delineated using multiple cut-off values (0–25 for sands/sandstones, 25–35 for silty sands/silty sandstones, 35–55 for silts, 55–60 for silty shales, 60–100 for shales).

The following stage was represented by the depth conversion of the TWT maps, in which the *Depth Map by Shared T-D Chart* function was applied. In order to avoid consistent errors that reached more than 600 m for the charts in the existent wells, due to low drilling depths, one pseudo-well was built using both the TWT and depth seismic surveys (Fig. 3). This approach presumed that each stratigraphic element (sea bottom, BSR, the top of the reservoir, Benioff zone etc.) from the time volume was assigned to the exact same element in the depth seismic.

The final approach in the methodology marked the integration of the results from the previous phases in order to define the petroleum systems and to establish a couple of prospects with their associated volumetric calculations.

4. HYDROCARBON POTENTIAL AND PETROLEUM SYSTEMS – RESULTS AND DISCUSSIONS

Two, fully imaged, elongated anticline structures (that are named in this paper Tokugawa and Toranaga) (Fig. 5), that have not been drilled yet, were selected for the evaluation of the hydrocarbon potential in the area. The biogenic gas system in the Nankai region was defined using core and log data from the COOO6 well and the interpretation from the seismic survey. The system includes the following elements:

- Source rocks: plant fragment-bearing silty and shaly turbidite levels. Hydrocarbons are definitely of microbial origin, due to the low heat flux values and temperatures in the area that make the thermogenic origin impossible. The existence of biogenic gas is demonstrated by the BSR reflector (Fig. 2), which is a consequence of the presence of gas hydrates (a cryogenized mixture of water and methane). Another indicator is represented by the high RMS Amplitude values obtained bellow the BSR map, suggesting the existence of free gases in the reservoirs under the gas hydrates;
- Traps: mostly structural (anticline folds with 3 way dip closure or 4 way dip closure);
- Seal: fine grained sedimentary intervals or the BSR level.
- Reservoir rocks: porous and permeable, high quality turbidite sandstones/sands;
- Migration pathways: the most important hydrocarbon migration occurs *in situ* in the basin floor fan sequences; another scenario is for the gas to circulate along thrust faults, but this process comes with a question mark, for two reasons (a, b): gas hydrates are present in the area, so they could act as a seal unit, decreasing the possibility of gas molecules to migrate along faults and fractures (a); there are no gas seepages that could indicate hydrocarbon leakages at the bottom of the ocean (b);

The results for the volumetric section were obtained in a special module of the Kingdom Program which runs the calculations. The main input consisted of the P90 and P10 statistic values for: the areal extent of the last closing contour, Net/Gross Ratio, porosity, water saturation, gas volume factor, gas recovery factor (Table 1).

Each polygon`s area was measured directly by the software (Fig. 6) and the Net-to-Gross Ration was obtained from the V_{sh} curve by using two endmembers from the COOO6 well (which is positioned close to the oceanic trench): the second and fourth tectono-stratigraphic units. The second unit in the borehole is characterized by a low NTG value, the sequence being dominated by thick shale intervals. Sandstone bodies are thin and non-amalgamated. This scenario corresponds to mud-rich submarine fan systems or to the overlap of distal areas of lobes in regular turbidites. On the other hand, the fourth unit is dominated almost exclusively by massive arenite deposits, suggesting a sand rich basin floor fan or multiple median lobe zones that are super imposed (Fig. 7).

Porosity values were available in the well final completion report. The rest of the parameters, such as the water saturation, gas volume factor and gas recovery factor, were evaluated with respect to the fluid type and the depth of the structure (related to pressure and temperature).

The recoverable resources (Table 2), as expressed by the P_{mean} values (the median between P99 and P1), are 600 BCF (billion cubic feet) for the Tokugawa Prospect and 291 BCF for the Toranaga Prospect. These results suggest that the area could pe economically profitable. A new exploration well can decipher the oil and gas potential in the imbricate nappes of the outer prism.

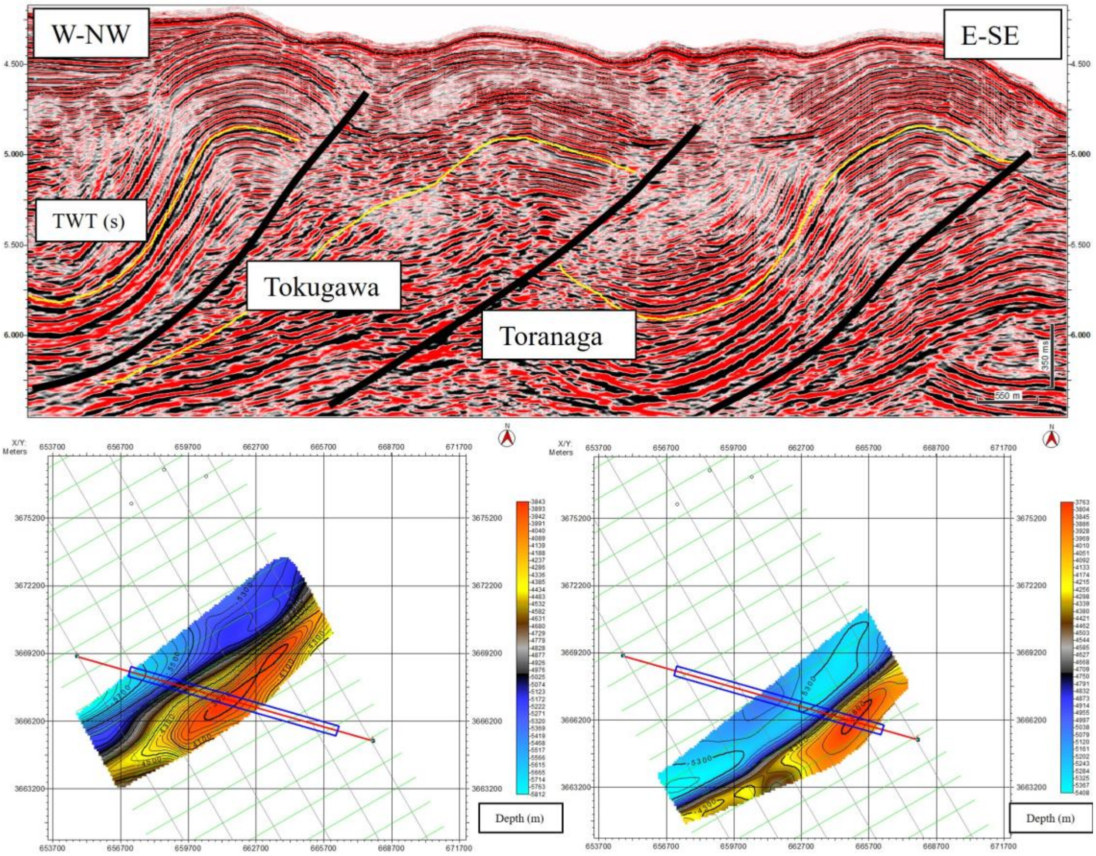

Fig. 5 – The two elongated anticline structures (Tokugawa on the left; Toranaga on the right) that have been evaluated for the biogenic gas potential, as seen from a seismic line and from the structural maps in depth.

Table 1

Input parameters for the volumetric calculations: last closing contours areas, NTG, porosity, water saturation, gas volume factor and gas recovery factor.

PARAMETER	LOWER LIMIT (P90)	UPPER LIMIT (P10)
Last closing contour for the Toranaga Prospect (square m)	619037	6599967
Last closing contour for the Tokugawa Prospect (square m)	627526	11198021
NTG	0.11	0.92
Porosity (ϕ)	0.3	0.38
Water saturation (Sw)	0.2	0.3
Gas volume factor (Bg) (SCF/ cu ft)	300	350
Gas recovery factor	0.75	0.8

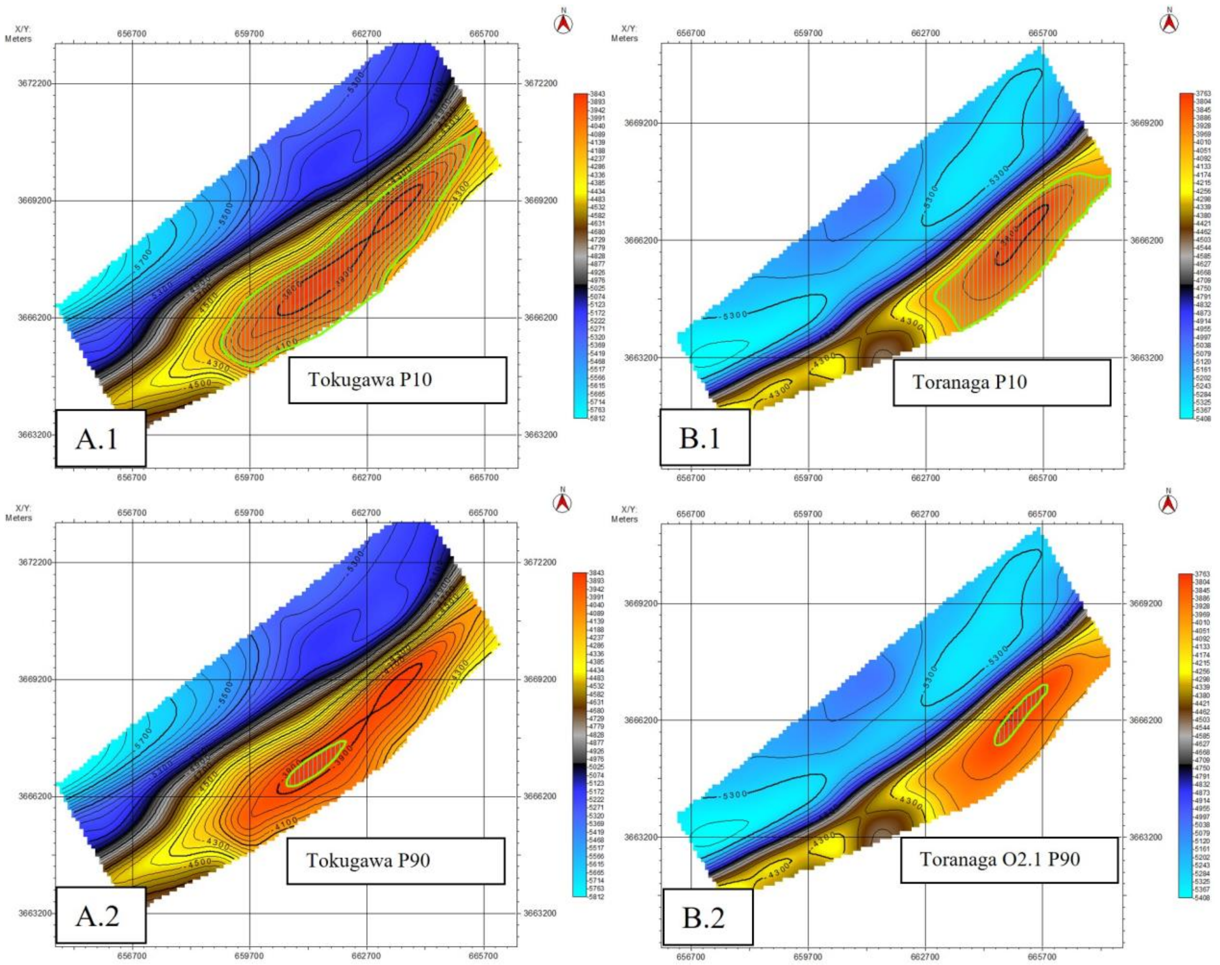

Fig. 6 – The last closing contours for the two structures in the statistic scenarios: P10 (A.1; B.1) and P90 (A.2; B.2).

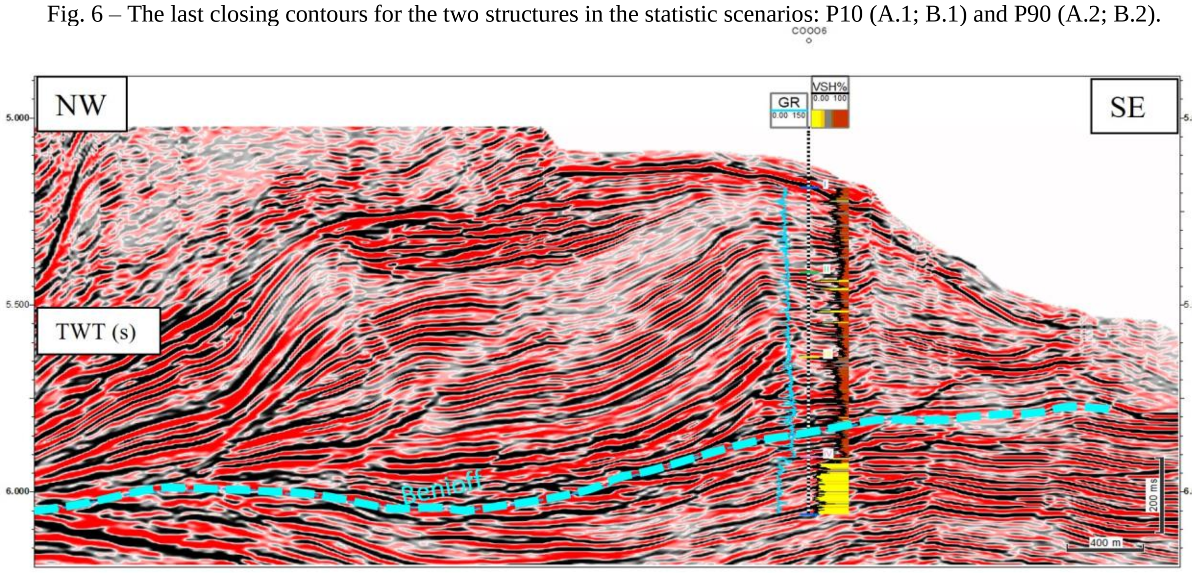

Fig. 7 – Seismic section and V_{sh} curve from the location of the COOO6 well.
The two endmembers for the NTG, units II and IV, can be observed.

Table 2

Recoverable resources from the two prospects in terms of statistic variations

Statistic variations	Tokugawa resources (BCF)	Toranaga resources (BCF)
P1	2581	1060
P10	1396	610
P50	436	222
P90	108	75
P99	32	20
Mean	617	291

5. CONCLUDING REMARKS

In this study we were able to define the petroleum system of the Nankai accretionary complex in the offshore area of southwest Japan using petrophysical, sedimentological and structural inferences from the seismic and well dataset. Every single element of the biogenic gas system was delineated over the course of the project: source rocks (shales and silts rich in organic matter), reservoirs (turbidite sandstones), migration (mostly in situ, but also possibly along thrusts), traps (structural) and seal (hemipelagic or turbidite shales).

The hydrocarbon volumes, as reffered from the P*mean* values of the statistical calculations, indicate that the Nankai subduction zone can be economically subject to exploration and production activities. The Tokugawa structure yields over 600 BCF of methane and Toranaga hosts almost 300 BCF of gas. For example, the premiere gas fields in the Western Black Sea Shelf, Ana and Doina, from the MGD Project operated by Black Sea Oil&Gas S.A., include a volume of 300 BCF (P50 value), smaller than the 436 BCF (P50 value) recoverable resources that were assumed for the Tokugawa Prospect.

Acknowledgments. The authors would like to thank the JAMSTEC Agency in Japan and the IODP for providing the dataset and IHS Markit for offering a free Kingdom license.

REFERENCES

BEAUMONT, C. (1981), *Foreland Basins*. Geophysical Journal International, 65, 291–329.

BOSTON, B., MOORE, G.F., JURADO, M.J., SONE, H. (2016), *Deformation of the Nankai Trough inner accretionary prism: the role of inherited structures*. Geochemistry, Geophysics, Geosystems, 17, 485–500.

CHAMOT-ROOKE, N., RENARD, V., LE PICHON, X. (1987), *Magnetic anomalies in the Shikoku Basin: A new interpretation*. Earth and Planetary Science Letters, 83, 214–228.

GULICK, S.P., BANGS, N.L., MOORE, G.F., ASHI, J., MARTIN, K.M., SAWYER, D.S., TOBIN, H.J., KURAMOTO, S., TAIRA, A. (2010). *Rapid forearc basin uplift and megasplay fault development from 3D seismic images of Nankai Margin off Kii Peninsula, Japan*. Earth and Planetary Science Letters, 300, 55–62.

HIBBARD, J., KARIG, D. (1990), *Alternative plate model for the early Miocene evolution of the southwest Japan margin*. Geology, 18, 170–174.

KIMURA, G., KITAMURA, Y., HASHIMOTO, Y., YAMAGUCHI, A., SHIBATA, T., UJIEE, K., OKAMOTO, S. (2007), *Transition of accretionary wedge structures around the up-dip limit of the seismogenic subduction zone*. Earth and Planetary Science Letters, 255, 471–484.

KIMURA, G., MOORE, G.F., STRASSER, M., SCREATON, E., CUREWITZ, D., STREIFF, C., TOBIN, H. (2011), *Spatial and temporal evolution of the megasplay fault in the Nankai Trough*. Geochemistry, Geophysics, Geosystems, 12.

KIMURA, G., HASHIMOTO, Y., KITAMURA, Y., YAMAGUCHI, A., KOGE, H. (2014), *Middle Miocene swift migration of the TTT triple junction and rapid crustal growth in southwest Japan: a review*. Tectonics, 33, 1219–1238.

MIYAZAKI, S.I., HEKI, K. (2001), *Crustal velocity field of southwest Japan: subduction and arc-arc collision*. Journal of Geophysical Research, 106, 4305–4326.

MOORE, G.F., BOSTON, B.B., STRASSER, M., UNDERWOOD, M.B., RATLIFF, R.A. (2015), *Evolution of tectono-sedimentary systems in the Kumano Basin, Nankai Trough forearc*. Marine and Petroleum Geology, 67, 604–616.

OKINO, K., SHIMAKAWA, Y., NAGAOKA, S. (1994), *Evolution of the Shikoku Basin*. Journal of Geomagnetism and Geoelectricity, 46, 463–479.

PARK, J.-O., TSURU, T., KODAIRA, S., CUMMINS, P.R., KANEDA, Y. (2002), *Splay fault branching along the Nankai subduction zone*. Science, 297, 1157–1160.

SAFFER, D., MCNEILL, L., ARAKI, E., BYRNE, T., EGUCHI, N., TOCZKO, S., TAKAHASHI, K. (2009), *NanTroSEIZE stage 2: NanTroSEIZE riser/riserless observatory*. IODP Preliminary Report 319.

SCREATON, E., KIMURA, G., CUREWITZ, D., MOORE, G.F., CHESTER, F., FABBRI, O., FERGUSSON, C., GIRAULT, F., GOLDSBY, D., HARRIS, R., INAGAKI, F., JIANG, T., KITAMURA, Y., KNUTH, M., LI, C.-F., CLAESSON LILJEDAHL, L., LOUIS, L., MILLIKEN, K., NICHOLSON, U., RIEDINGER, N., SAKAGUCHI, A., SOLOMON, E., STRASSER, M., SU, X., TSUTSUMI, A., YAMAGUCHI, A., UJIEE, K, ZHAO, X. (2009), *Interactions between deformation and fluids in the frontal thrust region of the NanTroSEIZE transect offshore the Kii Peninsula, Japan: results from IODP Expedition 316 Sites C0006 and C0007*. Geochemistry, Geophysics, Geosystems, 10.

SENO, T., MARUYAMA, S. (1984), *Paleogeographic reconstruction and origin of the Philippine Sea*. Tectonophysics, 102, 53–84.

SENO, T., STEIN, S., GRIPP, A.E. (1993), *A model for the motion of the Philippine Sea plate consistent with NUVEL-1 and geological data*. Journal of Geophysical Research, 98, 17941–17948.

SHIRAISHI, K., YAMANDA, Y., NIBE, T. (2019), *Thermogenic petroleum potential of the Nankai subduction zone, Offshore SW Japan*. Journal of Petroleum Geology, 42, 417–434.

STRASSER, M., MOORE, G.F., KIMURA, G., KITAMURA, Y., KOPF, A.J., LALLEMANT, S., PARK, J.-O., SCREATON, E.J., SU, X., UNDERWOOD, M.B., ZHAO, X. (2009), *Origin and evolution of a splay fault in the Nankai accretionary wedge*. Nature Geoscience, 2, 648–652.

UYEDA, S. (1981), *Subduction zones and back arc basins – A review*. Geologische Rundschau, 70, 552–569.

ZANG, S.X., CHEN, Q.Y., NING, J.Y., SHEN, Z.K., LIU, Y.G. (2002), *Motion of the Philippine Sea plate consistent with the NUVEL-1A model*. Geophysical Journal International, 150, 809–819.